IEEE Access
Multidisciplinary | Rapid Review | Open Access Journal

Date of publication xxxx 00, 0000, date of current version xxxx 00, 0000.

Digital Object Identifier 10.1109/ACCESS.2017.Doi Number

Time-and-Frequency Hybrid Multiplexing for Flexible Ambiguity Controls of DFT-coded MIMO OFDM Radar

JUNSEUK SUH[1], (Student Member, IEEE), JUNGAH LEE[2], GYE-TAE GIL[3], and SONGCHEOL HONG[1], (Member, IEEE)

[1]The Department of Electrical Engineering, Korea Advanced Institute of Science and Technology (KAIST). Daejeon 305-701, South Korea
[2]AURA Intelligent Systems, Boston, USA
[3]KAIST Institute (KI) for IT Convergence, KAIST 291, Daehak-ro, Yuseong-gu, Daejeon 305-338, South Korea

Corresponding author: Songcheol Hong (e-mail: schong1234@kaist.ac.kr).

This work was supported by a grant from the Institute of Information & Communications Technology Planning & Evaluation (IITP) funded by the Korean government (MSIT) (2019-0-00826, High resolution intelligent Radcomm system).

ABSTRACT A time-and-frequency hybrid multiplexing technique for a multiple-input multiple-output (MIMO) orthogonal frequency-division multiplexing (OFDM) radar is proposed. Discrete Fourier transform (DFT)-coded OFDM waveforms are introduced, which allow it to be free from range-dependent angle errors. These are readily used to provide both time-domain and frequency-domain multiplexings in the MIMO OFDM radar. The DFT-coded frequency-domain multiplexing shortens the maximum unambiguous range, while the DFT-coded time-domain multiplexing lowers the maximum Doppler ambiguity. A hybrid of both domain multiplexing techniques can mitigate the respective limitations by adaptively selecting the proper DFT matrix size in each multiplexing domain. This allows to solve the intrinsic range and Doppler ambiguity problems of MIMO radars by controlling the hybrid ratio of the two kinds of DFT-code based multiplexing methods. Range-Doppler and range-angle maps of four examples with different hybrid multiplexing ratios are simulated with a MIMO OFDM radar numerical platform.

INDEX TERMS Discrete Fourier transform (DFT) code, hybrid multiplexing, multiple-input multiple-output (MIMO) radar, orthogonal frequency-division multiplexing (OFDM) radar, range and Doppler ambiguities.

I. INTRODUCTION

Rapidly-growing attentions have been paid to automotive radar sensors over the past decade, as the cost of the hardware has drastically decreased with the advent of advanced semiconductor technologies. Better performance capabilities in range and angular resolutions of radar sensors are competitively required, as they are very important features not only to detect objects but also to recognize them in optical camera or light detection and ranging (LiDAR) applications [1]-[7]. Many antennas and transceiver chains in multiple-input multiple-output (MIMO) radar systems are necessary to obtain high angular resolutions, of which millimeter-wave front-ends are implemented often with multiple chipsets in a cascade form with appropriate local oscillator (LO) distributions [8]-[11]. Virtual receive array (VRA) methods are widely adopted to synthesize a large aperture size effectively for high angular resolution [2]-[17].

To implement a MIMO radar, the orthogonality among transmit signals has to be satisfied. As the number of transmitter (TX) components increases, it becomes more difficult to maintain orthogonality. To this end, time division multiplexing (TDM) [3]-[5], [14]-[16], frequency division multiplexing (FDM) [10], [17]-[19], and code division multiplexing (CDM) [20]-[22] have been applied to MIMO radars. Regarding the TDM method, because only one TX out of multiple TX paths transmits a signal at a particular time, this multiplexing method suffers from a loss of processing gain with respect to the number of TX antennas. Even though there is no bandwidth loss, both the motion-induced error problem [15]-[16], and the Doppler ambiguity limit can arise. In the case of FDM, because all TX paths operate simultaneously, there is no issue about Doppler ambiguity limit as increasing the number of TX antennas. However, given that the signal bandwidth is divided and

reduced, the range resolution is degraded. Also, a range-angle coupling problem occurs [17]-[19]. With regard to CDM, all of the above-mentioned disadvantages disappear, but unlike TDM and FDM, it is difficult to realize perfect orthogonality due to the cross-correlation property among the codes, which increases the noise floor and will limit the radar performance due to the reduced dynamic range during radar target detection.

On the other hand, digital-oriented MIMO radar systems employing phase-modulated continuous-wave (PMCW) signals [2], [12] or orthogonal frequency-division multiplexing (OFDM) signals [23]-[44] have been studied for next-generation automotive radar systems. The MIMO OFDM radar, which has many advantages such as proliferation of radio-frequency (RF) front-ends from communication system [29]-[30], flexible digital design [31]-[32], and interference mitigation [34]-[35] is expected to be widely used in a radar sensor network [36]-[37], passive radars [38]-[40], and joint radar-communication (JRC) [31]-[34], [41]-[44] as the fields of future technology. Since OFDM-based JRC systems are seriously considered to be promising digital radars, the OFDM waveforms have been intensively studied to further increase the communication capacity [41]-[42] or improve the range and Doppler resolutions of radars [43]-[44]. To use a VRA with MIMO OFDM radar, a spectrally interleaved MIMO multiplexing method for the orthogonality of TX signals is often employed in earlier studies [23]-[29]. It has the advantage of offering perfect orthogonality between the TX signals, and all TXs can operate simultaneously. However, a drawback in this case is that the maximum unambiguous range is reduced due to the large subcarrier spacing as the number of TX paths increases. In addition, because subcarriers allocated for TXs have frequency offsets equal to the subcarrier spacing, the implemented VRA has a range-dependent array response [28]. In order to solve this problem during spectrally interleaved MIMO multiplexing, an additional process to separate the angle information of each target according to the array response of a VRA from the radial distance information is required.

Meanwhile, given that the conventional multiplexing methods introduced here have their own advantages and disadvantages, a hybrid multiplexing method can be a good strategy. Its advantage is that it can flexibly determine the hybridizing ratio of two multiplexing methods to satisfy the performance requirements of a given radar system. In other words, hybrid multiplexing allows the use of a larger number of TXs while mitigating limitations due to the disadvantages of multiplexing techniques. In previous studies, a MIMO frequency-modulated continuous-wave (FMCW) radar system that applied time-and-frequency-division multiplexing was introduced [45]. However, it is difficult to change the hybrid multiplexing ratio adaptively because it needs to change the hardware configuration during the operation.

In this paper, a new hybrid multiplexing method suitable for a large number of TXs in a MIMO OFDM radar system is proposed. The TX signal can be multiplexed by multiplying discrete Fourier transform (DFT) matrices of appropriate sizes in the frequency-space domain as well as in the time-space domain. The proposed method allows to redefine the radar performances of the range and Doppler ambiguities by software during its operation according to user needs adaptively without changing the hardware configuration. Also, the adaptive control of the hybrid ratio by changing the DFT matrix sizes in time-space and frequency-space domains can allow to resolve the range and Doppler ambiguities simultaneously. The MIMO OFDM radar using DFT-coded OFDM waveforms is free from range-dependent angle errors, while the ones using a conventional spectrally interleaved multiplexing scheme are severely affected.

The remainder of this paper is arranged as follows. The signal structures of several multiplexing methods for a MIMO OFDM radar are described in Section II. In Section III, the proposed DFT-coded time-and-frequency hybrid multiplexing method is presented with the explanation of a system architecture and a radar signal model. In addition, the theoretical analysis of the proposed multiplexing method is presented in this section. Then, simulations using a numerical computing tool (MATLAB) to verify the multiplexing idea are presented, and their performance analysis is explained in Section IV. Finally, the conclusion is drawn in Section V.

II. SIGNAL STRUCTURES OF MIMO OFDM RADAR

A. CONVENTIONAL METHOD WITH SPECTRALLY INTERLEAVED MIMO

First of all, an OFDM radar signal transmitted in a single TX is represented as $x_{\mathrm{TX}}(t)$, which can be expressed by

$$x_{\mathrm{TX}}(t) = \sum_{m=0}^{M-1} \sum_{n=0}^{N-1} D(n,m) \exp(\mathrm{j}2\pi f_n t) \cdot \mathrm{rect}\left(\frac{t - mT_{\text{radar pulse}}}{T_{\text{radar pulse}}}\right), \quad (1)$$

where $f_n = n \cdot \Delta f \left(= \frac{n}{T_{\text{OFDM symbol}}}\right)$, N is the number of subcarriers, and n refers to the index of the subcarrier. Also, M denotes the number of coherent radar pulses, m is the index of the OFDM symbol, and $T_{\text{radar pulse}}$ represents the duration of the radar pulse. f_n refers to the frequency of each subcarrier, and $\mathrm{rect}(t/T_{\text{radar pulse}})$ denotes the rectangular window function with the duration of $T_{\text{radar pulse}}$ in the time domain. $D(n,m)$ refers to the element of the n^{th} subcarrier and m^{th} OFDM symbol with complex random payload data, and Δf is the subcarrier spacing and must satisfy the reciprocal of the OFDM symbol period, $T_{\text{OFDM symbol}}$.

Meanwhile, the conventional multiplexing method is described in Fig. 1 with that of the widely used spectrally interleaved MIMO scheme. The multiplexing procedure is

This article has been accepted for publication in a future issue of this journal, but has not been fully edited. Content may change prior to final publication. Citation information: DOI 10.1109/ACCESS.2021.3117980, IEEE Access

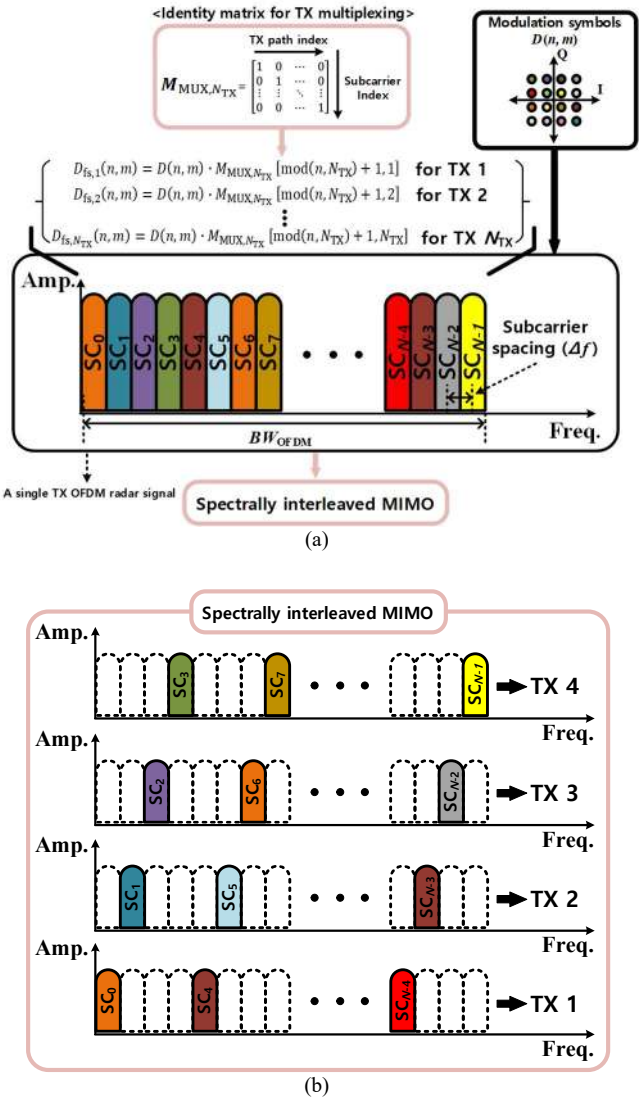

FIGURE 1. MIMO OFDM radar signal structures in the frequency domain: (a) Multiplexing procedure for MIMO OFDM radar with a corresponding multiplexing matrix (an identity matrix in this case) and (b) TX signals with the spectrally interleaved MIMO multiplexing. Four TXs are assumed in this figure.

represented in the frequency domain in Fig. 1(a). The above-mentioned method is one type of the matrix applied for multiplexing in the frequency-space domain. $\boldsymbol{M}_{\mathrm{MUX},N_{\mathrm{TX}}}$ refers to the multiplexing matrix with the size of N_{TX} x N_{TX} to generate the signals of N_{TX} transmitters and $M_{\mathrm{MUX},N_{\mathrm{TX}}}[\alpha,\beta]$ accordingly represents an element located in α^{th} row and β^{th} column. Basically, the m^{th} OFDM symbol is presented in the frequency domain in Fig. 1(a), in which payload data with different colors are allocated to N subcarriers. SC_n denotes the n^{th} subcarrier component, and BW_{OFDM}, i.e., the entire OFDM signal bandwidth, is obtained as $N{\cdot}\Delta f$.

The frequency-space domain multiplexed signals, such as the spectrally interleaved multiplexing and the DFT-coded frequency-domain multiplexing which is introduced in Section II - B, can be described in the same form. $n_{\mathrm{TX}}^{\mathrm{th}}$ TX signal is referred to $x_{\mathrm{TXs,fs},n_{\mathrm{TX}}}(t)$, and is expressed by

$$x_{\mathrm{TXs,fs},n_{\mathrm{TX}}}(t)=\sum_{m=0}^{M-1}\sum_{n=0}^{N-1}D_{\mathrm{fs},n_{\mathrm{TX}}}(n,m)\exp(\mathrm{j}2\pi f_n t)\cdot\mathrm{rect}\left(\frac{t-mT_{\mathrm{radar\ pulse}}}{T_{\mathrm{radar\ pulse}}}\right), \quad (2a)$$

where

$$D_{\mathrm{fs},n_{\mathrm{TX}}}(n,m)=D(n,m)\cdot M_{\mathrm{MUX},N_{\mathrm{TX}}}[\mathrm{mod}(n,N_{\mathrm{TX}})+1,n_{\mathrm{TX}}], \quad (2b)$$

and $D_{\mathrm{fs},n_{\mathrm{TX}}}(n,m)$ in (2b), which is represented in Fig. 1(a) denotes the multiplexed payload data in the $n_{\mathrm{TX}}^{\mathrm{th}}$ frequency-space domain for the n^{th} subcarrier and m^{th} OFDM symbol. Also, mod(x, y) denotes the remainder of x divided by y in (2b). For the spectrally interleaved MIMO, an identity matrix is applied as $\boldsymbol{M}_{\mathrm{MUX},N_{\mathrm{TX}}}$. Accordingly, the spectrally interleaved MIMO multiplexing can be done through an element-wise multiplication of the payload data allocated to each subcarrier and the identity matrix in the frequency-space domain for all OFDM symbols as shown in this figure. Along the procedure of the pink circled parts in Fig. 1(a), as the rows and columns of a 4 x 4 identity matrix are considered as the subcarrier index and TX path index, respectively, all subcarriers can be alternately allocated to four TXs by matching the TX path index to the remainder of the subcarrier index divided by four, as in earlier work [29]. For the example of four multiplexed TX signals in a MIMO OFDM radar using the conventional method is shown in Fig. 1(b).

B. DFT-CODED FREQUENCY-DOMAIN MIMO AND TIME-DOMAIN MIMO

The signal of the DFT-coded frequency-domain MIMO is also expressed by the same equation of (2a), except for a DFT matrix which is applied as $\boldsymbol{M}_{\mathrm{MUX},N_{\mathrm{TX}}}$. Instead of using an identity matrix, if a 4 x 4 DFT matrix is used along the procedure of the pink circled parts in Fig. 1(a), DFT-coded multiplexing is achieved. In this multiplexing scheme, all of the TX signals include all subcarrier components, but each TX signal is obtained by multiplying a DFT matrix with original payload data for every OFDM symbol in the frequency domain. Fig. 2(a) shows the signal structure of the four DFT-coded frequency-domain multiplexed TX signals in the time domain. The rows and columns of a 4 x 4 DFT matrix are considered as the subcarrier index and TX path index, respectively. The multiplexing can be done through an element-wise multiplication of the payload data allocated to each subcarrier and the DFT matrix as explained with the green circled parts in Fig. 2(a).

A pulse used in an OFDM radar consists of a cyclic prefix (CP) with the period of T_{cp} and an OFDM symbol with the period of $T_{\mathrm{OFDM\ symbol}}$. By adding a CP in front of that OFDM symbol as a guard time, the round-trip time delay of a certain target within the maximum detectable distance can be retrieved without an inter-symbol interference (ISI) issue in an OFDM radar. Due to the characteristic of the DFT matrix applied in the frequency domain, each TX signal shows circular shift characteristics in the time domain. While S_m denotes to time-domain samples of the m^{th} OFDM symbol,

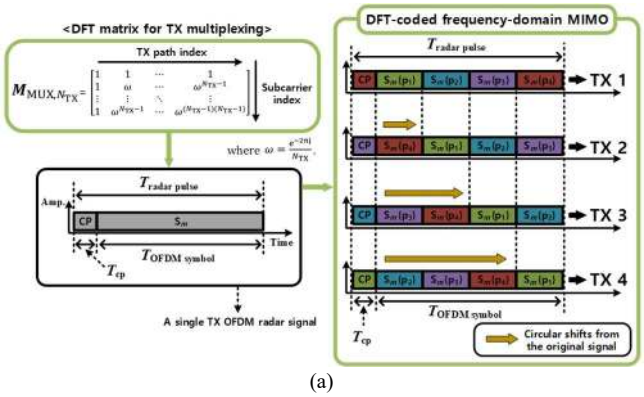

(a)

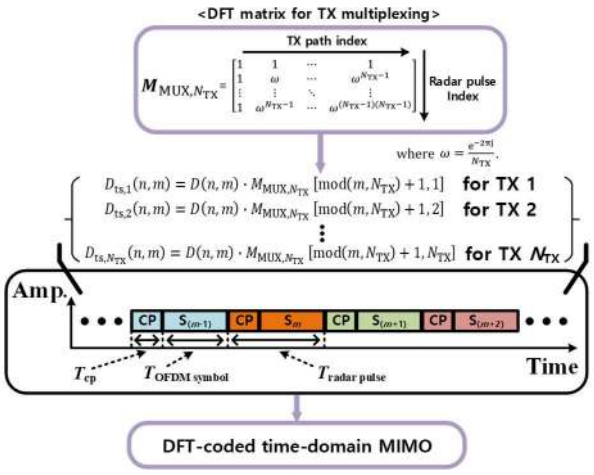

(b)

FIGURE 2. MIMO OFDM radar signal structures in the time domain: (a) DFT-coded frequency-domain MIMO multiplexing and (b) DFT-coded time-domain MIMO multiplexing. Four TXs are assumed to each multiplexing method in this figure.

$S_m\{p_1\}$ to $S_m\{p_4\}$ represent time-domain samples obtained by dividing the OFDM symbol into four equal divisions on the time axis as shown in this figure. Although the signals with the DFT-coded frequency-domain MIMO are multiplexed with the same OFDM symbol, different CPs are required due to the different operations of the circular shifting for each TX.

On the other hand, the multiplexing of DFT-coded time-domain MIMO method is represented along the procedure of the purple circled parts in Fig. 2(b). As the four time-domain multiplexed TX signals are assumed in this figure, 4 x 4 DFT matrix is used in radar pulses. The rows and columns of the matrix are considered as the radar pulse index and TX path index, respectively. The signals of a DFT-coded time-domain MIMO OFDM radar for the multiple TXs can be readily described by expanding (1). The DFT-coded time-domain multiplexed n_{TX}^{th} TX signal is referred to $x_{TXs,ts,n_{TX}}(t)$, and is expressed by

$$x_{TXs,ts,n_{TX}}(t) = \sum_{m=0}^{M-1}\sum_{n=0}^{N-1} D_{ts,n_{TX}}(n,m)\exp(j2\pi f_n t) \cdot \mathrm{rect}\left(\frac{t-mT_{radar\ pulse}}{T_{radar\ pulse}}\right), \quad (3a)$$

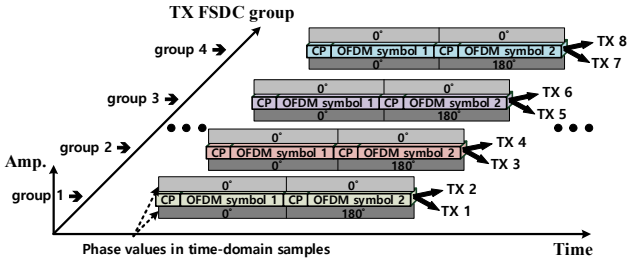

FIGURE 3. Structures of the proposed DFT-coded time-and-frequency hybrid multiplexing MIMO OFDM radar signals in the time domain. For a simple explanation, eight TXs with 4 x 4 DFT-coded frequency-domain MIMO and 2 x 2 DFT-coded time-domain MIMO are assumed in this figure.

where

$$D_{ts,n_{TX}}(n,m) = D(n,m) \cdot M_{MUX,N_{TX}}[\mathrm{mod}(m,N_{TX})+1,n_{TX}] \quad . \quad (3b)$$

In (3b), $D_{ts,n_{TX}}(n,m)$, which is represented in Fig. 2(b) denotes the multiplexed payload data in the n_{TX}^{th} time-space domain for the n^{th} subcarrier and m^{th} OFDM symbol. Also, a DFT matrix is applied as $\boldsymbol{M}_{MUX,N_{TX}}$ in this case. As described in (3a) and (3b), the multiplexing in the time-space domain can be achieved through an element-wise multiplication of the time-domain samples in consecutive n_{TX} radar pulses with the DFT matrix for all subcarriers. This procedure is similar to a Doppler division multiplexing (DDM) method in the MIMO radar approaches described in earlier studies [46]-[47]. To obtain the orthogonality in the Doppler domain, successive radar pulses as many as the number of multiplexed TXs are required. For the case that the same OFDM symbol is repeated in certain successive radar pulses, each CP should be required between these OFDM symbols in the multiplexed signals with DFT-coded time-domain MIMO due to each phase shifting operation.

III. PROPOSED MULTIPLEXING METHOD OF MIMO OFDM RADAR

A. PROPOSED DFT-CODED TIME-AND-FREQUENCY HYBRID MIMO

The proposed DFT-coded time-and-frequency hybrid multiplexing MIMO method can be achieved with the combination of the DFT-coded frequency-domain MIMO scheme and the DFT-coded time-domain MIMO scheme. In other words, DFT-coded frequency-domain MIMO scheme described in Fig. 2(a) can be extended to the proposed DFT-coded time-and-frequency hybrid multiplexing MIMO scheme by additionally applying a DFT matrix in the time-space domain described in Fig. 2(b). These primarily multiplexed signals in the frequency domain create four frequency-space DFT coded (FSDC) signal groups which are the input of the proposed DFT-coded time-and-frequency hybrid multiplexing method.

The signal structure of this proposed multiplexing is illustrated in the time domain as shown in Fig. 3. In terms of FSDC signal groups which are the primarily multiplexed

signals in the frequency domain, each group is applied to an additional time-domain multiplexing through element-wise multiplications with a 2 x 2 DFT matrix. Accordingly, because a 4 x 4 DFT matrix is applied in the frequency-space domain and the 2 x 2 DFT matrix is applied in the time-space domain, eight TX signals are generated by the hybrid multiplexing technique, as an example with the hybrid multiplexing ratio of 4 : 2 shown in this figure.

To describe the proposed method in detail, the system architecture and the radar signal model are explained. The transmitter architecture of the proposed DFT-coded time-and-frequency hybrid multiplexing MIMO OFDM radar is shown in Fig. 4(a). A DFT matrix multiplier block for frequency-space multiplexing is introduced onto a conventional OFDM radar transmitter described in earlier study [30], and the other matrix multiplier blocks for time-space multiplexing are also utilized along the respective transmitting paths. The sizes of the two types of DFT-coded multiplexing matrices are denoted as $N_{\mathrm{TX,fs}}$ and $N_{\mathrm{TX,ts}}$, respectively. The OFDM radar signal is primarily multiplexed into $N_{\mathrm{TX,fs}}$ TX FSDC groups. Each TX FSDC group is again multiplexed by multiplying an $N_{\mathrm{TX,ts}}$ x $N_{\mathrm{TX,ts}}$ element-wise DFT matrix in the time-space domain such that $N_{\mathrm{TX,fs}} \cdot N_{\mathrm{TX,ts}}$ of TXs in total can be operated.

The general signal model of the proposed DFT-coded time-and-frequency hybrid MIMO OFDM radar for the multiple TXs can be obtained by combining (2a) and (3a). The proposed DFT-coded hybrid multiplexed signal in the $n_{\mathrm{fs}}^{\mathrm{th}}$ frequency-space domain and $m_{\mathrm{ts}}^{\mathrm{th}}$ time-space domain is referred to $x_{\mathrm{TXs},n_{\mathrm{fs}},m_{\mathrm{ts}}}(t)$, and is expressed by

$$x_{\mathrm{TXs},n_{\mathrm{fs}},m_{\mathrm{ts}}}(t) = \sum_{m=0}^{M-1}\sum_{n=0}^{N-1} D(n,m)\, A_{\mathrm{fs}}(n,n_{\mathrm{fs}}) \cdot \exp(\mathrm{j}2\pi f_n t)\, A_{\mathrm{ts}}(m,m_{\mathrm{ts}})\, \mathrm{rect}\left(\frac{t-mT_{\mathrm{radar\ pulse}}}{T_{\mathrm{radar\ pulse}}}\right), \quad (4)$$

where

$$A_{\mathrm{fs}}(n,n_{\mathrm{fs}}) = M_{\mathrm{DFT},N_{\mathrm{TX,fs}}}\left[\mathrm{mod}\left(n,N_{\mathrm{TX,fs}}\right)+1,n_{\mathrm{fs}}\right], \quad (5a)$$

$$A_{\mathrm{ts}}(m,m_{\mathrm{ts}}) = M_{\mathrm{DFT},N_{\mathrm{TX,ts}}}\left[\mathrm{mod}\left(m,N_{\mathrm{TX,ts}}\right)+1,m_{\mathrm{ts}}\right]. \quad (5b)$$

$\boldsymbol{M}_{\mathrm{DFT},N_{\mathrm{TX,fs}}}$, a DFT matrix applied in the frequency-space domain, and $\boldsymbol{M}_{\mathrm{DFT},N_{\mathrm{TX,ts}}}$, a DFT matrix applied in the time-space domain, are introduced in (4). Each n_{fs} and m_{ts} refers path index multiplexed in the frequency domain and the time domain, respectively. In (5a), $A_{\mathrm{fs}}(n,\ n_{\mathrm{fs}})$ is the element of $\boldsymbol{M}_{\mathrm{DFT},N_{\mathrm{TX,fs}}}$ with respect to n and n_{fs} as described in Fig. 2(a). Also in (5b), $A_{\mathrm{ts}}(m,\ m_{\mathrm{ts}})$ is the element of $\boldsymbol{M}_{\mathrm{DFT},N_{\mathrm{TX,ts}}}$ with respect to m and m_{ts} as described in Fig. 2(b). These two elements are multiplied in an element-wise manner to obtain DFT-coded TX signals. The signal models for a MIMO OFDM radar with the several above-introduced multiplexing methods can be unified with (4), in which only the applied matrices are differed for each multiplexing scheme.

On the other hand, the receiver (RX) architecture of the MIMO OFDM radar is shown in Fig. 4(b). Unlike the transmitter structure, multiplier blocks of inverse discrete Fourier transform (IDFT) matrices for de-multiplexing in the frequency-space and time-space domains are introduced onto a conventional OFDM radar receiver [30]. Since the de-multiplexing process is achieved in the reverse order of the multiplexing in TX, RX time-space DFT coded (TSDC) groups which are the primarily de-multiplexed signals in the time-space domain are generated as many as $N_{\mathrm{TX,ts}}$, and each RX TSDC group is applied to an additional frequency-domain de-multiplexing through element-wise multiplications with a $N_{\mathrm{TX,fs}}$ x $N_{\mathrm{TX,fs}}$ IDFT matrix. Finally, all target-reflected signals from each TX antenna can be separated in each RX antenna. While n^{th} RX antenna component is referred to n_{RX}, the received MIMO OFDM radar signals in n_{RX}, $y_{n_{\mathrm{RX}},\mathrm{TXs}}(t)$ is expressed by

$$y_{n_{\mathrm{RX}},\mathrm{TXs}}(t) = \alpha_k \sum_{k=1}^{K_{\mathrm{target}}} x_{\mathrm{TXs},n_{\mathrm{fs}},m_{\mathrm{ts}}}(t-\tau_k) = \sum_{k=1}^{K_{\mathrm{target}}}\sum_{m_{\mathrm{ts}}=1}^{N_{\mathrm{TX,ts}}}\sum_{n_{\mathrm{fs}}=1}^{N_{\mathrm{TX,fs}}}\sum_{m=0}^{M-1}\sum_{n=0}^{N-1} \alpha_k D(n,m)\, A_{\mathrm{fs}}(n,n_{\mathrm{fs}}) \cdot \exp\left(\mathrm{j}2\pi f_n(t-\tau_k)\right) A_{\mathrm{ts}}(m,m_{\mathrm{ts}})\, \mathrm{rect}\left(\frac{(t-\tau_k)-mT_{\mathrm{radar\ pulse}}}{T_{\mathrm{radar\ pulse}}}\right), \quad (6)$$

where

$$\tau_k = \frac{2(R_k+v_k t)+\left(\left((m_{\mathrm{ts}}-1)N_{\mathrm{TX,fs}}+n_{\mathrm{fs}}-1\right)N_{\mathrm{RX}}+n_{\mathrm{RX}}-1\right)d\sin\theta_k}{c_0}. \quad (7)$$

K_{target} denotes the total number of targets, and k refers to the index of targets at this time. While α_k denotes the attenuation factor of k^{th} target, τ_k represents a monostatic round-trip time delay of k^{th} target, which contains the radial distance, R_k, the radial velocity, v_k, and the path difference between TX antennas and RX antennas from the position of k^{th} target, θ_k. In (7), c_0 represents the speed of light, and the number of total RX antennas is referred to N_{RX}. The TX antennas are spaced apart by the total extent of the RX antennas, where d refers to RX antenna spacing. After the removal of CP, the MIMO OFDM radar signals in the frequency domain can be obtained through the fast Fourier transform (FFT) processing, for which $n_{\mathrm{fs}}^{\mathrm{th}}$ frequency-space domain DFT de-multiplexed and $m_{\mathrm{ts}}^{\mathrm{th}}$ time-space domain DFT de-multiplexed signals are expressed by

$$Y_{n_{\mathrm{RX}},n_{\mathrm{fs}},m_{\mathrm{ts}}}(n,m) \approx \sum_{k=1}^{K_{\mathrm{target}}}\sum_{m_{\mathrm{ts}}=1}^{N_{\mathrm{TX,ts}}}\sum_{n_{\mathrm{fs}}=1}^{N_{\mathrm{TX,fs}}}\sum_{m=0}^{M-1}\sum_{n=0}^{N-1} \alpha_k\, D(n,m) \cdot A_{\mathrm{fs}}(n,n_{\mathrm{fs}})\, B_{\mathrm{fs}}(n,n_{\mathrm{fs}})\, A_{\mathrm{ts}}(m,m_{\mathrm{ts}})\, B_{\mathrm{ts}}(m,m_{\mathrm{ts}}) \cdot \exp\left(\mathrm{j}\frac{2\pi}{\lambda}\phi_{k,n_{\mathrm{fs}},m_{\mathrm{ts}},n_{\mathrm{RX}}}\right)\exp\left(-\mathrm{j}2\pi f_n \tau_{k,R}\right) \cdot \exp\left(\mathrm{j}2\pi f_{k,d} m T_{\mathrm{radar\ pulse}}\right) + Z(n,m), \quad (8)$$

where

$$\phi_{k,n_{\mathrm{fs}},m_{\mathrm{ts}},n_{\mathrm{RX}}} = \frac{\left(\left((m_{\mathrm{ts}}-1)N_{\mathrm{TX,fs}}+n_{\mathrm{fs}}-1\right)N_{\mathrm{RX}}+n_{\mathrm{RX}}-1\right)d\sin\theta_k}{c_0}, \quad (9)$$

and

This article has been accepted for publication in a future issue of this journal, but has not been fully edited. Content may change prior to final publication. Citation information: DOI 10.1109/ACCESS.2021.3117980, IEEE Access

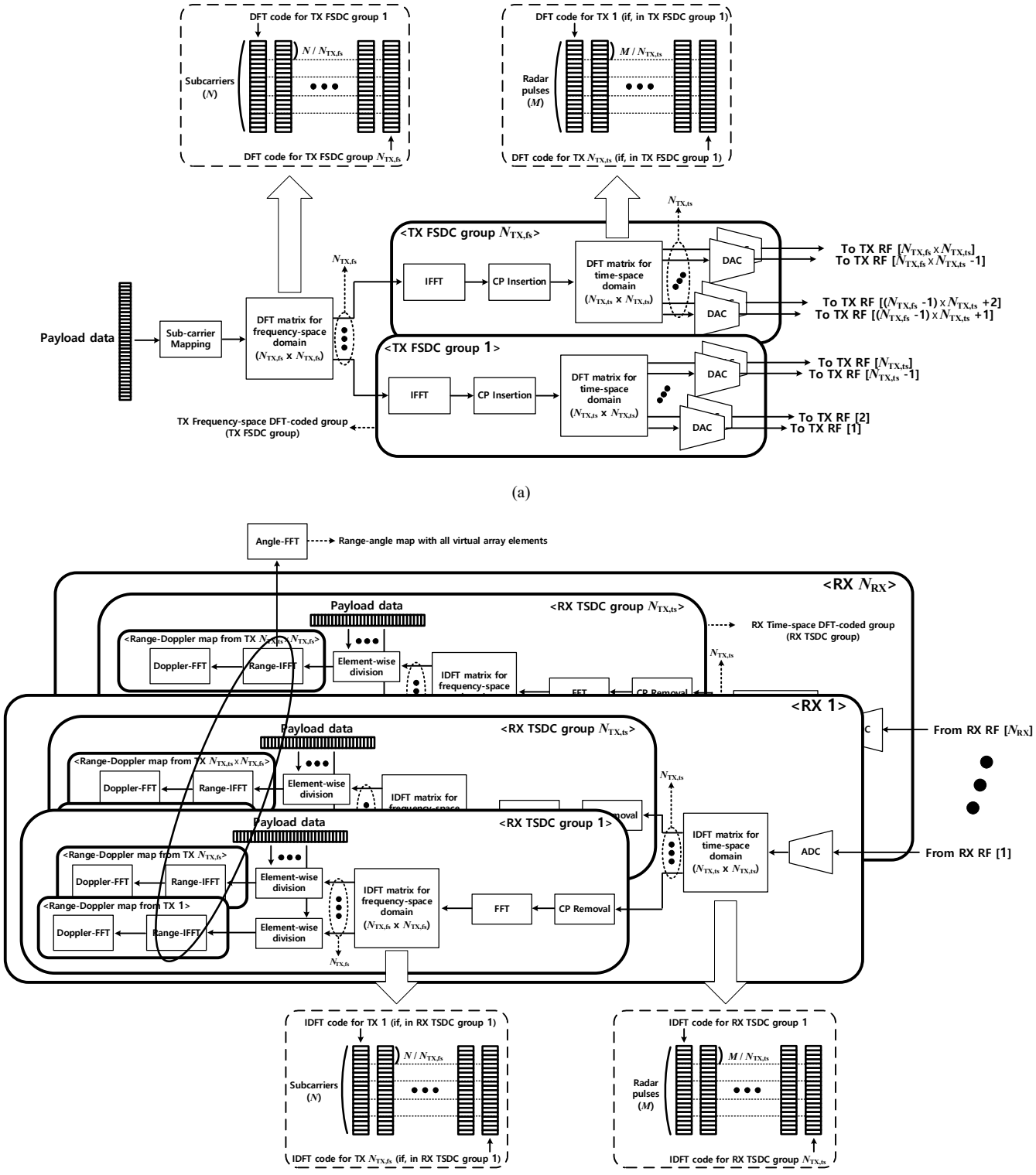

FIGURE 4. **Architecture of the proposed DFT-coded time-and-frequency hybrid multiplexing MIMO OFDM radar: (a) multiple TXs, (b) multiple RXs.**

$$B_{\mathrm{fs}}(n, n_{\mathrm{fs}}) = M_{\mathrm{IDFT},N_{\mathrm{TX,fs}}}\left[\mathrm{mod}\left(n, N_{\mathrm{TX,fs}}\right) + 1, n_{\mathrm{fs}}\right] , \quad (10a)$$

$$B_{\mathrm{ts}}(m, m_{\mathrm{ts}}) = M_{\mathrm{IDFT},N_{\mathrm{TX,ts}}}\left[\mathrm{mod}\left(m, N_{\mathrm{TX,ts}}\right) + 1, m_{\mathrm{ts}}\right] . \quad (10b)$$

In (10a), $B_{\mathrm{fs}}(n, n_{\mathrm{fs}})$ is the element of $\boldsymbol{M}_{\mathrm{IDFT},N_{\mathrm{TX,fs}}}$ which is the Hermitian form of (5a) with respect to n and n_{fs}. Also in (10b), $B_{\mathrm{ts}}(m, m_{\mathrm{ts}})$ is the element of $\boldsymbol{M}_{\mathrm{IDFT},N_{\mathrm{TX,ts}}}$ which is the Hermitian

form of (5b) with respect to m and m_{ts}. Under the assumption of ignoring the phase terms related to the range-Doppler coupling, (7) can be obviously classified into different exponential terms with $\tau_{k,R} = \frac{2R_k}{c_0}$, $f_{k,d} = \frac{2v_k}{c_0} f_{\mathrm{c}}$ in (8), and $\phi_{k,n_{\mathrm{fs}},m_{\mathrm{ts}},n_{\mathrm{RX}}}$ in (9). λ represents the wavelength of a radar carrier frequency, and $Z(n, m)$ denotes additive complex white Gaussian noise in (8).

The radar channel information which contains the delay due to the radial distance, Doppler component, and angle of the target, is retrieved by element-wise divisions with a symbol of the known transmitted payload data. The payload data symbol is originally used to generate the total number ($N_{\mathrm{TX,fs}} \cdot N_{\mathrm{TX,ts}}$) of TX signals in the proposed multiplexing scheme. All of these signals are received by one receiver and passed through each element-wise division block. This gives the channel information from the $N_{\mathrm{TX,fs}} \cdot N_{\mathrm{TX,ts}}$ TX chains. The second exponential term and the third exponential term in (8) are expressed by

$$h_{k,R}(n) = \exp\left(-\mathrm{j}2\pi n \Delta f \tau_{k,R}\right), \tag{11}$$

and

$$h_{k,d}(m) = \exp\left(-\mathrm{j}2\pi m T_{\text{radar pulse}} f_{k,d}\right), \tag{12}$$

respectively, so that the range and Doppler information is readily obtained by the post signal processing approaches such as range inverse fast Fourier transform (IFFT) along the subcarrier axis and Doppler FFT along the OFDM symbol axis. The range information of k^{th} target from a certain TX can be expressed by

$$r_k(\eta_k) = \mathrm{IDFT}\left[h_{k,R}(n)\right] = \frac{1}{N}\sum_{n=0}^{N-1} h_{k,R}(n)\exp\left(\mathrm{j}\frac{2\pi}{N} n\eta_k\right), \tag{13}$$

where $\eta = 0, \ \ldots, N-1$. A peak will occur at the index of η_k at

$$\eta_k = \left\lfloor \tau_{k,R} \Delta f N \right\rceil . \tag{14}$$

In a similar way, the velocity information of k^{th} target can be expressed by

$$V_k(\zeta_k) = \mathrm{DFT}\left[h_{k,d}(m)\right] = \frac{1}{M}\sum_{m=0}^{M-1} h_{k,d}(m)\exp\left(-\mathrm{j}\frac{2\pi}{M} m\zeta_k\right), \tag{15}$$

where $\zeta = 0, \ \ldots, M-1$. A peak will occur at the index of ζ_k at

$$\zeta_k = \left\lfloor \frac{2v_k f_c T_{\text{radar pulse}} M}{c_0} \right\rceil . \tag{16}$$

Subsequently, $N_{\mathrm{TX,fs}} \cdot N_{\mathrm{TX,ts}}$ range-Doppler maps are obtained. A range-angle map is also achieved from the final MIMO VRA which is obtained by extending the radar channel information with several coherent RXs. Angle FFT along the VRA axis can be used to determine the angle information of the target.

B. ANALYSIS OF THE PROPOSED TECHNIQUE

1) FLEXIBLE CONTROL OF RANGE AND DOPPLER AMBIGUITIES

In terms of the range and Doppler ambiguity performance of the proposed hybrid multiplexing method, DFT-coded frequency-domain MIMO scheme has an influence on the range ambiguity while DFT-coded time domain MIMO scheme has an influence on the Doppler ambiguity of radar performance. $T_{\text{OFDM symbol}}$ determines the unambiguous range of R_{unamb} as considered from (11), which can be applied as

$$R_{\mathrm{unamb}} = \frac{c_0 \, T_{\text{OFDM symbol}}}{2 \, N_{\mathrm{TX,fs}}} , \tag{17}$$

where R_{unamb} is divided by $N_{\mathrm{TX,fs}}$ in the DFT-coded frequency-domain MIMO. The de-multiplexing process of multiple TX signals in the frequency domain occurs this range ambiguity degradation. The presented range of target with the ambiguity, R'_k can be expressed by

$$R'_k(p_{\mathrm{r},k}) = R_k - p_{\mathrm{r},k} R_{\mathrm{unamb}} , \quad \text{for } R'_k > 0 \tag{18}$$

where $p_{\mathrm{r},k}$ is a positive integer including zero, a value with the number of repetition cycles for the range ambiguity of the k^{th} target. For the specific value in the desired unambiguous range region, $p'_{\mathrm{r},k}$ is expressed by

$$p'_{\mathrm{r},k} = \arg\min_{p_{\mathrm{r},k}} (R'_k) . \tag{19}$$

Thus, the estimated range of the k^{th} target in the desired unambiguous region is referred to $\bar{R}_k$ ($= R'_k(p'_{\mathrm{r},k})$), and it is shown in the result from the obtained range-Doppler map and range-angle map.

However, a radar with the DFT-coded time-domain MIMO method has the performance of the Doppler ambiguity degradation due to the de-multiplexing process of multiple TX signals in the time domain. It should be noted that $T_{\text{radar pulse}}$ determines the unambiguous velocity of v_{unamb} as considered from (12). This can be written as

$$v_{\mathrm{unamb}} = \frac{c_0}{4 \, f_c \, T_{\text{radar pulse}} N_{\mathrm{TX,fs}}} . \tag{20}$$

In this case, v_{unamb} is divided by $N_{\mathrm{TX,ts}}$. This is similar to the result of the DDM method, because the number of minimum coherent pulses is determined to maintain the TX orthogonality in the Doppler-space domain. The presented velocity of target with the ambiguity, v'_k can be expressed by

$$v'_k(p_{\mathrm{v},k}) = \begin{cases} v_k - 2p_{\mathrm{v},k} v_{\mathrm{unamb}} , & \text{if } v_k > 0 \\ v_k + 2p_{\mathrm{v},k} v_{\mathrm{unamb}} , & \text{if } v_k < 0 \end{cases} \tag{21}$$

where $p_{\mathrm{v},k}$ is a positive integer including zero, a value with the number of repetition cycles for the velocity ambiguity of the k^{th} target. For the specific value in the desired unambiguous velocity region, $p'_{\mathrm{v},k}$ is expressed by

This article has been accepted for publication in a future issue of this journal, but has not been fully edited. Content may change prior to final publication. Citation information: DOI 10.1109/ACCESS.2021.3117980, IEEE Access

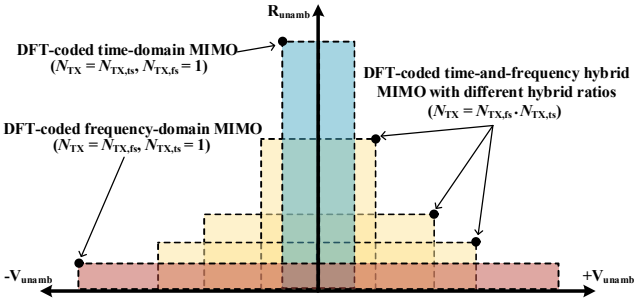

FIGURE 5. Theoretical range-Doppler unambiguous area of the proposed hybrid multiplexing method in the range-Doppler plane. This is determined by the hybrid ratio of two multiplexing methods, which is ($N_{TX,fs}$: $N_{TX,ts}$). Here, the number of TXs is N_{TX} = $N_{TX,fs}$ · $N_{TX,ts}$.

$$p'_{v,k} = \arg\min_{p_{v,k}}(|v'_k|) \ . \tag{22}$$

Thus, the estimated velocity of the k^{th} target in the desired unambiguous region is referred to $\bar{v}_k$ $(= v'_k(p'_{v,k}))$, and it is shown in the result from the obtained range-Doppler map.

Meanwhile, a radar with the proposed hybrid multiplexing method offers an advantage compared to those with spectrally interleaved MIMO schemes in that range and Doppler ambiguities can be controlled according to the needs of the radar performance. For the case of the spectrally interleaved MIMO method which is similar to the DFT-coded frequency-domain MIMO method, it has the performance of the range ambiguity degradation as shown in (17). As the number of TXs increases, the range ambiguity also decreases so that wrong radar detection may occur when observing a distant target. But, the proposed hybrid multiplexing method alleviates this ambiguity problem even with a large number of TXs. Provided that the product of $N_{TX,fs}$ and $N_{TX,ts}$ equals to N_{TX}, the size of the DFT matrices in each domain can be flexibly adjusted according to the performance requirements of the radar. In other words, the hybrid multiplexing ratio can be determined to negotiate the maximum unambiguous range and velocity. To describe this ambiguity trade-off, the theoretical range-Doppler unambiguous area of the proposed hybrid multiplexing method is illustrated in Fig 5. It is expected to resolve the range and Doppler ambiguities simultaneously by controlling the hybrid ratio adaptively. After trial radar operations with all possible hybrid ratios in successive coherent pulse intervals (CPI)s, it is able to find whether an interested target is located in range and Doppler ambiguities or not; thereby, the particular performances of the radar can be adaptively improved according to time-varying demands. The simulated results about the range and Doppler ambiguity controls are shown in Section IV.

2) RANGE-DEPENDENT ANGLE ERRORS

As another advantage of the proposed hybrid multiplexing technique, the multiplexing method does not depend on the types of payload data, and all of the TXs operate with full BW_{OFDM} at the same time such that there are no range resolution loss as well as a processing gain loss in the MIMO OFDM radar. Also, while the DFT-coded time-and-frequency hybrid MIMO scheme preserves the original payload data with only phase value difference in each subcarrier and each OFDM symbol, the spectrally interleaved MIMO scheme generates frequency offsets of Δf along every transmitter as described in Fig. 1(b). Accordingly, a radar with the proposed MIMO scheme offers the other advantage compared to those with spectrally interleaved MIMO schemes in that range-dependent angle errors for each target do not occur in a range-angle map. For the simple comparison, the DFT-coded frequency-domain MIMO method is analyzed with the spectrally interleaved MIMO method since the both have a common feature of multiplexing in the frequency domain. As the range and angle information is the dyadic product of two each vector, the conventional MIMO virtual array beamforming vector, $\boldsymbol{F}(\theta)$, with respect to the number of TXs and RXs can be expressed by

$$\boldsymbol{F}(\theta) = \left[1,\ e^{j2\ \frac{d\sin\theta}{\lambda}}, e^{j2\pi\frac{2d\sin\theta}{\lambda}}, \dots, e^{j2\pi\frac{(N_{TX}N_{RX}-1)d\sin\theta}{\lambda}}\right]^{T} \ . \tag{23}$$

In (23), θ is the azimuth angle spanning from $-90°$ to $90°$, and superscript 'T' denotes transpose. As described in (13), the range compressed signal vector from a DFT-coded frequency-domain MIMO OFDM radar, $\boldsymbol{y}_{rc,DCF}(\tau)$, can be written as

$$\boldsymbol{y}_{rc,DCF}(\tau) = \left[y_{rc,DCF,0}(\tau), y_{rc,DCF,1}(\tau),\ \dots, y_{rc,DCF,(N_{TX}N_{RX}-1)}(\tau)\right] \ , \tag{24}$$

where $\tau\ (=\frac{2R}{c_0})$ refers to a round-trip time delay, R is a monostatic distance of a certain target. $\boldsymbol{y}_{rc,DCF}$ can be the same as $\boldsymbol{y}_{rc,MISO}$, which is the range compressed signal vector from a multiple-input single-output (MISO) OFDM radar with a $N_{TX}\cdot N_{RX}$ physical receiver array under the following condition:

$$\boldsymbol{y}_{rc,DCF}(\tau) = \boldsymbol{y}_{rc,MISO}(\tau), \quad \text{if } \tau < \frac{T_{OFDM\ symbol}}{N_{TX,fs}} \tag{25}$$

where $N_{TX,fs}$ refers to the DFT matrix with the size of $N_{TX,fs}$ x $N_{TX,fs}$ to generate the signals of $N_{TX,fs}$ transmitters in the frequency-space domain.

However, the range compressed signal vector from a spectrally interleaved MIMO OFDM radar, $\boldsymbol{y}_{rc,SI}$, can be also expressed under the same condition according to the size of an identity matrix. But, it contains another phase factor as a function of Δf. This is because subcarriers are alternately allocated to TXs with the period determined by the number of TXs in the spectrally interleaved MIMO scheme. With the approximation that Δf and BW_{OFDM} are much smaller than the carrier frequency, the phase difference, $\Delta\varphi$, between the subcarriers of a different $n_{TX,fs}^{\text{th}}$ TX with reference to the last TX as $N_{TX,fs}^{\text{th}}$ TX, for τ is expressed by

$$\Delta\varphi(n_{TX,fs}, \tau) = 2\pi\Delta f\tau(N_{TX,fs} - n_{TX,fs} - 1) \ . \tag{26}$$

For the consideration of all $\Delta\varphi$ according to each TX, $\boldsymbol{y}_{rc,SI}$ can be expressed as

$$\boldsymbol{y}_{rc,SI}(\tau) = \boldsymbol{y}_{rc,DCF}(\tau) \odot e^{j\Delta f(\boldsymbol{U}\otimes\boldsymbol{L})\tau} \ , \tag{27}$$

This article has been accepted for publication in a future issue of this journal, but has not been fully edited. Content may change prior to final publication. Citation information: DOI 10.1109/ACCESS.2021.3117980, IEEE Access

TABLE 1. Comparisons with multiplexing methods of MIMO OFDM radar for radar performance

Radar performance	Spectrally interleaved MIMO	DFT-coded frequency-domain MIMO	DFT-coded time-domain MIMO	DFT-coded time-and-frequency hybrid MIMO
Range-dependent angle errors	*$(0, 2\pi)$ during $\frac{R_{\text{unamb,ini}}}{N_{\text{TX,fs}}}$	Not affected.	Not affected.	Not affected.
Range ambiguity (R_{unamb})	$\frac{R_{\text{unamb,ini}}}{N_{\text{TX,fs}}}$	$\frac{R_{\text{unamb,ini}}}{N_{\text{TX,fs}}}$	Not affected.	Negotiable ($N_{\text{TX,fs}}$: $N_{\text{TX,ts}}$).
Doppler ambiguity (v_{unamb})	Not affected.	Not affected.	$\frac{v_{\text{unamb,ini}}}{N_{\text{TX,ts}}}$	

* If, $N_{\text{TX,fs}}$ is equal to two, phase errors occur within $(0, \pi)$.

where $\boldsymbol{U} = [0, 1, \ldots, N_{\text{TX}} - 1]^{\text{T}}$, and $\boldsymbol{L}$ is all-one vector with length N_{RX}. In (27), $\odot$ refers to the Hadamard (element-wise) product, and $\otimes$ denotes the Kronecker product. As described in (27), the additional phase factor causes range-dependent angle errors in a range-angle map of a MIMO radar. It is noted that the phase difference of the received signal in a certain RX from different TXs has periodicity of an unambiguous range, which is due to the range-angle coupling. Thus, it depends on how close a target is located at the integral multiple distances of the unambiguous range. In other words, the angle error of the k^{th} target depends on $\bar{R}_k$ which is derived by (18) and (19). As the number of TXs increases, the angle error in the range-angle map also increases, even with a slight change in the distance. With (23) and (24), the angular compressed signal from a DFT-coded frequency-domain MIMO OFDM radar, $\boldsymbol{y}_{\text{rc,ac,DCF}}$, can be written as

$$\boldsymbol{y}_{\text{rc,ac,DCF}}(\tau, \theta) = \boldsymbol{y}_{\text{rc,DCF}}(\tau)\, \boldsymbol{F}(\theta)^{\text{T}}. \tag{28}$$

To obtain a radar image, the FFT based digital beamforming can be simply applied, and the simulated results are shown with the comparison of the spectrally interleaved MIMO method in Section IV.

As the aspect of the range-dependent angle errors and the range and Doppler ambiguities in a MIMO OFDM radar, the summary about the changes of radar performance with the number of TXs is expressed in Table 1. In this comparison, $N_{\text{TX,fs}}$ refers to the number of TX paths multiplexed in the frequency-space domain, and $N_{\text{TX,ts}}$ denotes the number of TX paths multiplexed in the time-space domain. Also, the initial range and Doppler ambiguities are denoted as $R_{\text{unamb,ini}}$ and $v_{\text{unamb,ini}}$, respectively.

IV. MIMO OFDM RADAR SIMULATION

A. SIMULATION ENVIRONMENT

To verify the proposed multiplexing method for MIMO OFDM radar, a MATLAB simulation platform based on the transmitter and receiver architectures described in Section III is designed. The parameter values used for the radar simulation are shown in Table II. The number of TX and RX antennas of a MIMO radar to form a VRA are set to be 16 and 8, respectively. The antenna array of the MIMO radar for the VRA is shown in Fig. 6(a), and $*$ denotes a convolution. The RX antenna elements are spaced at $\lambda/2$, and the TX period becomes 4λ, which corresponds to the total size of the RX antenna array. A virtual receiver array with an aperture size of 64λ is formed, and an angular resolution close to 0.8° can be obtained theoretically. In Fig. 6(b), the array factor of the VRA is calculated with the antenna array geometry above. The grating lobes caused by the widely spaced TX antennas are canceled by the null points of the RX antenna array factor. As a result, a highly peaked array factor can be obtained with the VRA, and the peak gain is 42.14 dB $(= 20 \log_{10}(N_{\text{TX}} \cdot N_{\text{RX}}))$ with an isotropic antenna element pattern.

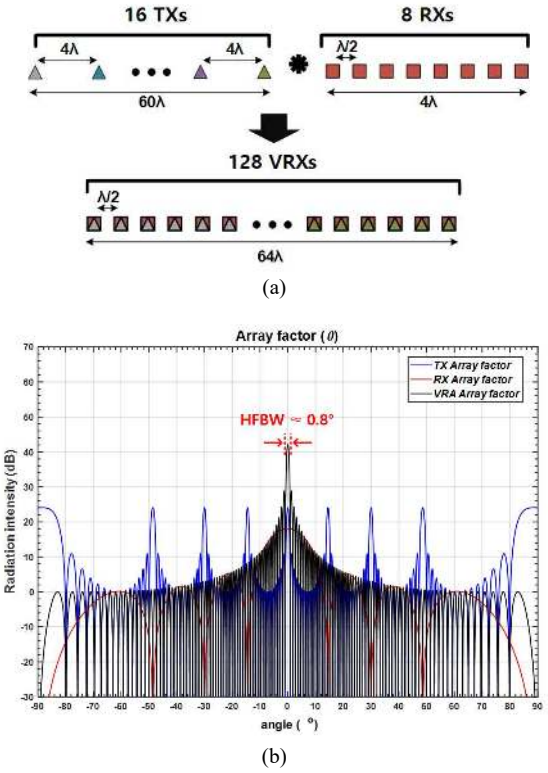

FIGURE 6. Antenna geometry and the array factor simulation for the 16 TXs and 8 RXs MIMO OFDM radar: (a) antenna array for the virtual receiver array and (b) array factor simulation for the virtual receiver array.

To show the characteristics of the proposed hybrid multiplexing radar, four different hybrid ratios of $N_{\text{TX,fs}} : N_{\text{TX,ts}}$ are set to be 16 : 1, 2 : 8, 8 : 2, and 4 : 4, and the simulation results are analyzed. Here, the product of $N_{\text{TX,fs}}$ and $N_{\text{TX,ts}}$ becomes the same number as N_{TX} of 16. A bandwidth of 2.048 GHz with a carrier frequency (f_c) of 79 GHz is assumed in the simulations. It is set to use 128 coherent radar pulses (M) for 320 μs, and a pulse duration ($T_{\text{radar pulse}}$) consists of a CP length (T_{cp}) of 0.5 μs and an OFDM symbol period ($T_{\text{OFDM symbol}}$) of 2 μs without OFDM symbol repetition. The MIMO OFDM radar simulation platform with sampling frequency (f_s) of 2.048 GHz produces a range-Doppler map and a range-angle map. The FFT size (N_{FFT}) for signal processing to obtain a range-Doppler map and a range-angle map is set to be 2048 x

This article has been accepted for publication in a future issue of this journal, but has not been fully edited. Content may change prior to final publication. Citation information: DOI 10.1109/ACCESS.2021.3117980, IEEE Access

TABLE 2. Parameters for the MIMO OFDM radar simulation

Parameter	Value	Remark	
Number of TX and RX antennas (N_{TX}, N_{RX})	TX : 16 RX : 8	Hybrid multiplexing ratio ($N_{TX,fs}$: $N_{TX,ts}$)	16 : 1 (in Fig. 7 case)
			2 : 8 (in Fig. 9 case)
			8 : 2 (in Fig. 10 case)
			4 : 4 (in Fig. 11 case)
Coherent radar pulses (M)	128	320 μs (=M $T_{radar\ pulse}$)	
Number of subcarriers (N)	4096		
Subcarrier spacing (Δf)	500 kHz		
Total OFDM bandwidth (BW_{OFDM})	2.048 GHz	Range resolution : 7.32 cm	
OFDM symbol period ($T_{OFDM\ symbol}$)	2 μs		
Unambiguous range (R_{unamb})	300 m	18.75 m (in Fig. 7 case)	Related to DFT-coded frequency-domain MIMO
		150 m (in Fig. 9 case)	
		37.5 m (in Fig. 10 case)	
		75 m (in Fig. 11 case)	
CP length (T_{cp})	0.5 μs	75 m : Maximum detectable range	
Unambiguous velocity (v_{unamb})	± 379.75 m/s	± 379.75 m/s (in Fig. 7 case)	Related to DFT-coded time-domain MIMO
		± 47.47 m/s (in Fig. 9 case)	
		± 189.88 m/s (in Fig. 10 case)	
		± 94.94 m/s (in Fig. 11 case)	
Carrier frequency (f_c)	79 GHz		

256, and the Taylor window is applied in the results for the uniformly distributed random payload data of 16-Qaudrature amplitude modulation (QAM). The simulations are assumed that all TXs and all RXs are synchronized, and the mismatch between chains is not considered. But, free-space path losses over target distances and additive white Gaussian noise (AWGN) are taken into consideration.

The arbitrarily assumed target information includes a radar cross-section (RCS), a range, a radial velocity, and an angle as shown in Table III. In the Simulation type 1, the only DFT-coded frequency-domain MIMO multiplexing is applied, where the hybrid multiplexing ratio is set to be 16 : 1. Four equidistant point targets with the same RCS and angle as described in Table III are used to show the dependency between range and angle, and its simulation result is shown in Fig. 7. In addition, the spectrally interleaved MIMO multiplexing with the same environment is also simulated in Fig. 8 for the comparisons.

TABLE 3. Target information for the simulation

Simulation type	n^{th} target	RCS (dBm^2)	Range (m)	Velocity (m/s)	Angle (°)
1 (Figs. 7-8)	1	-10	4	0	-30
	2	-10	6	0	-30
	3	-10	8	0	-30
	4	-10	10	0	-30
2 (Figs. 9-12)	1	-15	15	-54	0
	2	-12	37.75	0	-23.41
	3	-8	53.7	24.21	39.28

Furthermore, to verify the range and Doppler ambiguity controls of the proposed hybrid multiplexing scheme, the Simulation type 2 with three targets is performed. Figs. 9 to 12 show the range-Doppler map and range-angle map of the MIMO OFDM radar with the same geometry of a VRA in 16 TXs and 8 RXs. In Fig. 9, the hybrid multiplexing ratio of frequency-domain and time-domain MIMO is 2 : 8, and in Fig. 10, the ratio is 8 : 2. Finally, in Fig. 11, the ratio is 4 : 4. To compare the performances of the multiplexing methods, the simulation results of the spectrally interleaved MIMO multiplexing are also shown in Fig. 12.

B. SIMULATION RESULTS

A MIMO OFDM radar, which can support a VRA with 16 TXs and 8 RXs, is simulated with the only DFT-coded frequency-domain MIMO scheme. As shown in Fig. 7, the unambiguous velocity is not reduced, but the unambiguous range decreases by 1/16 in the range-Doppler map. Accordingly, a false signal from the first target appears at 22.75 m in the map, which is over the unambiguous range of 18.75 m. In the case of the spectrally interleaved MIMO multiplexing, simulations with 16 TXs and 8 RXs show the similar results in the range-Doppler map from Figs. 8(a) and (c). The unambiguous range also decreases by the same amount. As shown in Figs. 7(b) and (d), the equidistant targets set to be at $-30°$ show signals at the correct locations in the range-angle map. This means that the coupling between range and angle information does not occur with the DFT-coded frequency-domain MIMO multiplexing.

However, the same equidistant targets are plotted at the incorrect locations in the range-angle map for the case of the spectrally interleaved MIMO as shown in Figs. 8(b) and (d). The right-tilted angle information is due to the frequency offsets of subcarriers for every TX as described in (27). Since the range-angle coupling errors are closely related to the unambiguous range, an OFDM radar with the spectrally interleaved MIMO is not so good to operate a large number of TX antennas.

Meanwhile, as shown in Figs. 9 to 11, the maximum unambiguous range and the unambiguous velocity vary according to the hybrid multiplexing ratio. In Fig. 9, the first target is not at the maximum unambiguous velocity but the third target is in the maximum unambiguous range.

This article has been accepted for publication in a future issue of this journal, but has not been fully edited. Content may change prior to final publication. Citation information: DOI 10.1109/ACCESS.2021.3117980, IEEE Access

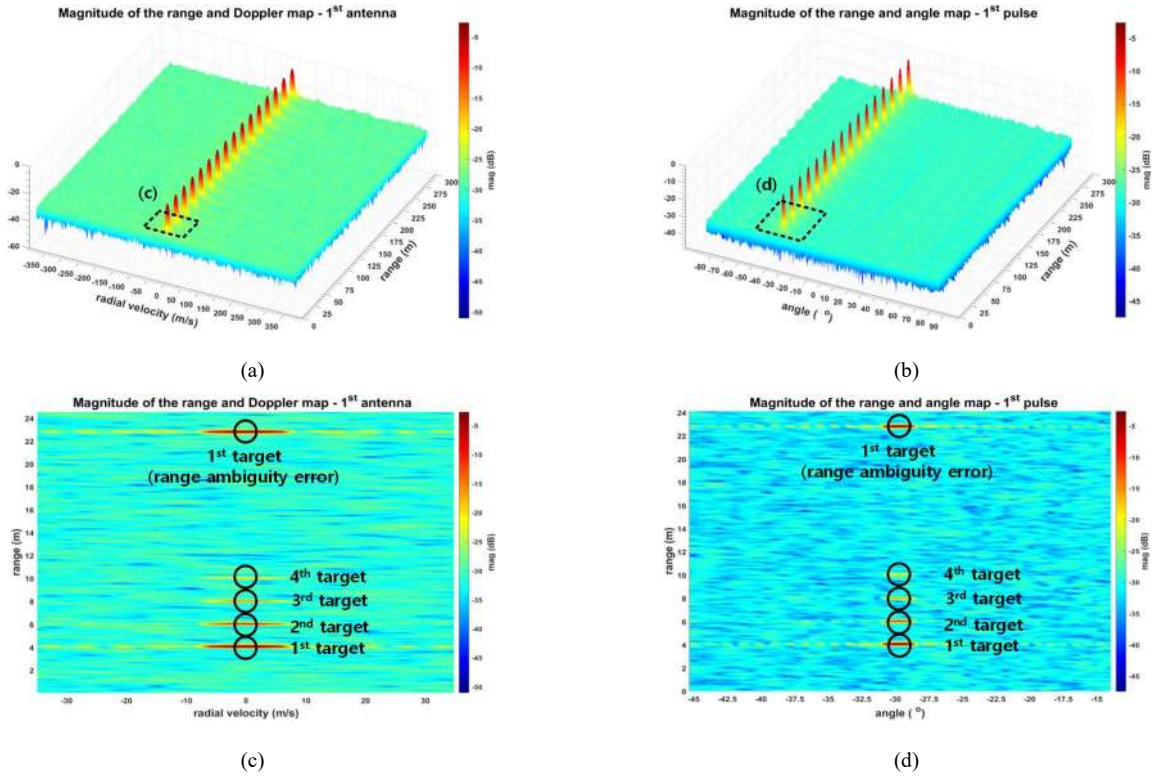

FIGURE 7. Simulation results of the 16 TXs & 8 RXs MIMO OFDM radar with the only DFT-coded frequency-domain MIMO: (a) range-Doppler map of a 3D view, (b) range-angle map of a 3D view, (c) range-Doppler map of a 2D view in detail (the dotted rectangle in (a)), and (d) range-angle map of a 2D view in detail (the dotted rectangle in (b)).

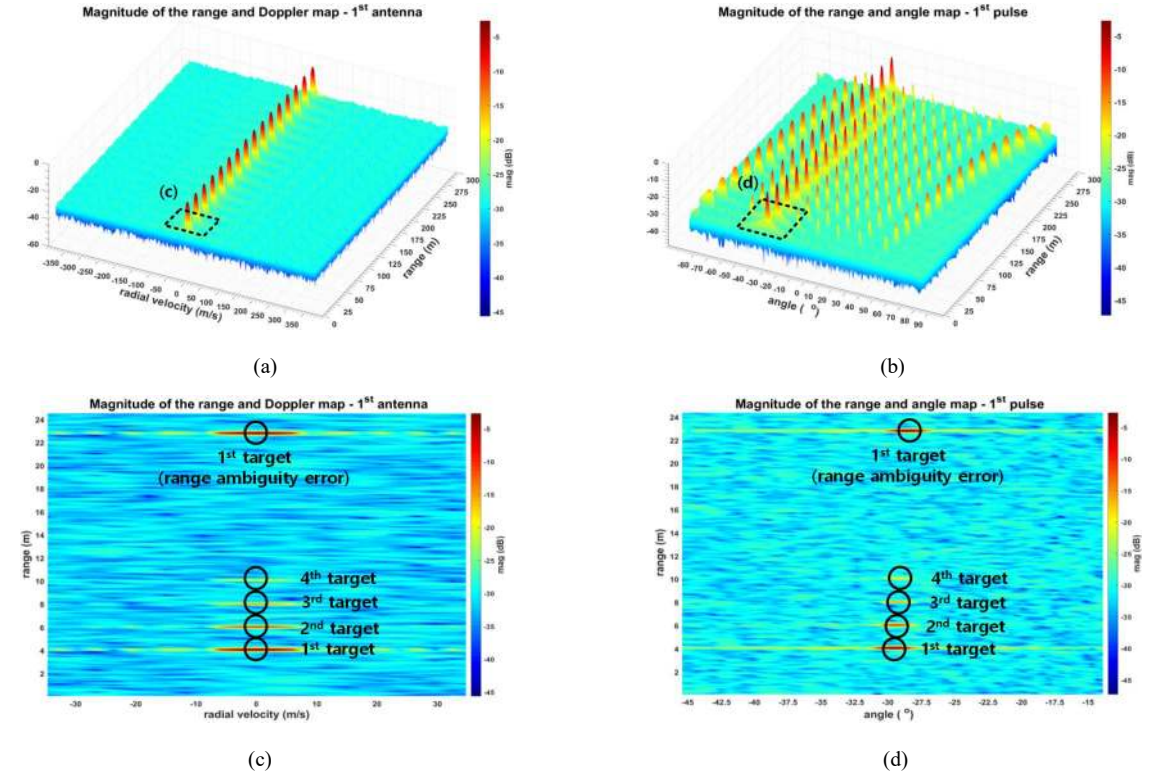

FIGURE 8. Simulation results of the 16 TXs & 8 RXs MIMO OFDM radar with the spectrally interleaved MIMO: (a) range-Doppler map of a 3D view, (b) range-angle map of a 3D view, (c) range-Doppler map of a 2D view in detail (the dotted rectangle in (a)), and (d) range-angle map of a 2D view in detail (the dotted rectangle in (b)).

This article has been accepted for publication in a future issue of this journal, but has not been fully edited. Content may change prior to final publication. Citation information: DOI 10.1109/ACCESS.2021.3117980, IEEE Access

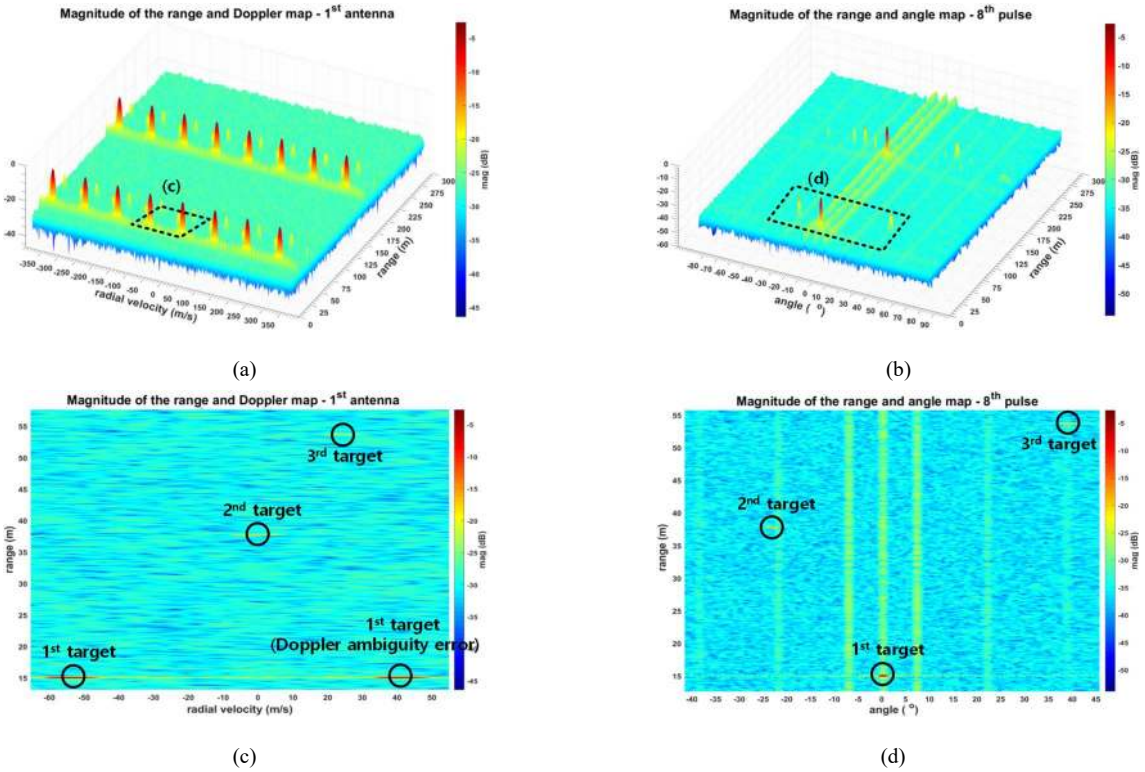

FIGURE 9. Simulation results of the 16 TXs & 8 RXs MIMO OFDM radar with 2 x 2 DFT-coded frequency-domain MIMO and 8 x 8 DFT-coded time-domain MIMO: (a) range-Doppler map of a 3D view, (b) range-angle map of a 3D view, (c) range-Doppler map of a 2D view in detail (the dotted rectangle in (a)), and (d) range-angle map of a 2D view in detail (the dotted rectangle in (b)).

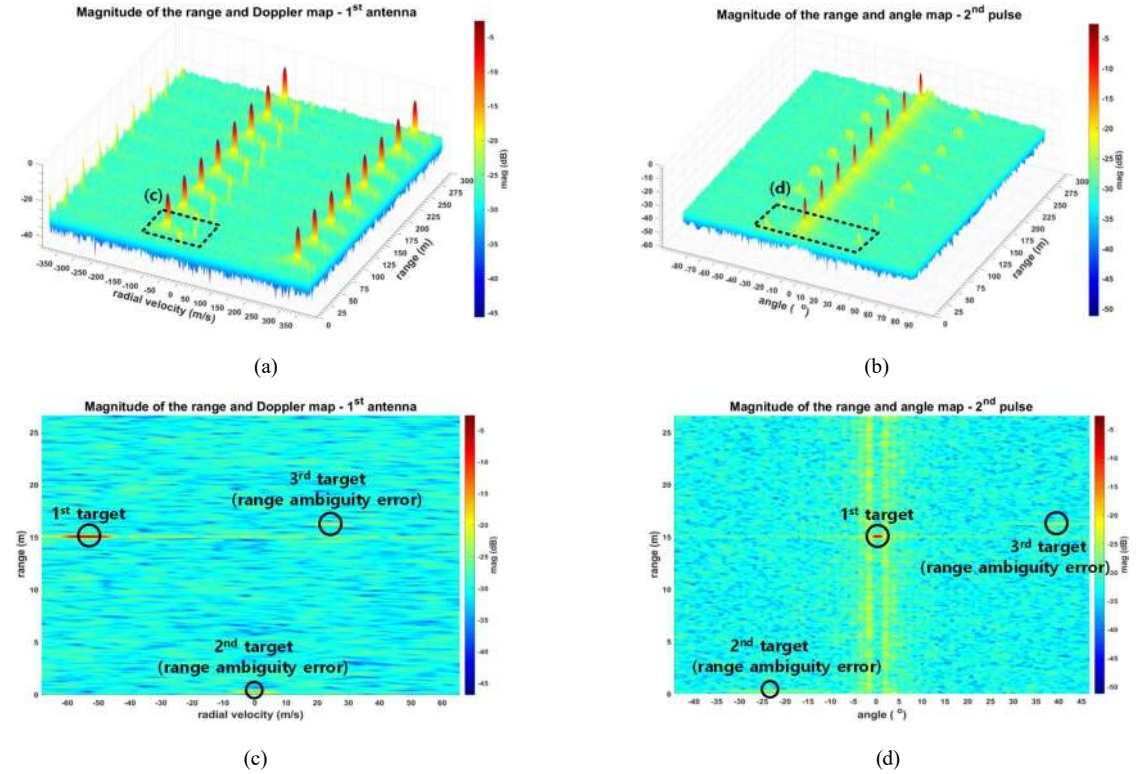

FIGURE 10. Simulation results of the 16 TXs & 8 RXs MIMO OFDM radar with 8 x 8 DFT-coded frequency-domain MIMO and 2 x 2 DFT-coded time-domain MIMO: (a) range-Doppler map of a 3D view, (b) range-angle map of a 3D view, (c) range-Doppler map of a 2D view in detail (the dotted rectangle in (a)), and (d) range-angle map of a 2D view in detail (the dotted rectangle in (b)).

This article has been accepted for publication in a future issue of this journal, but has not been fully edited. Content may change prior to final publication. Citation information: DOI 10.1109/ACCESS.2021.3117980, IEEE Access

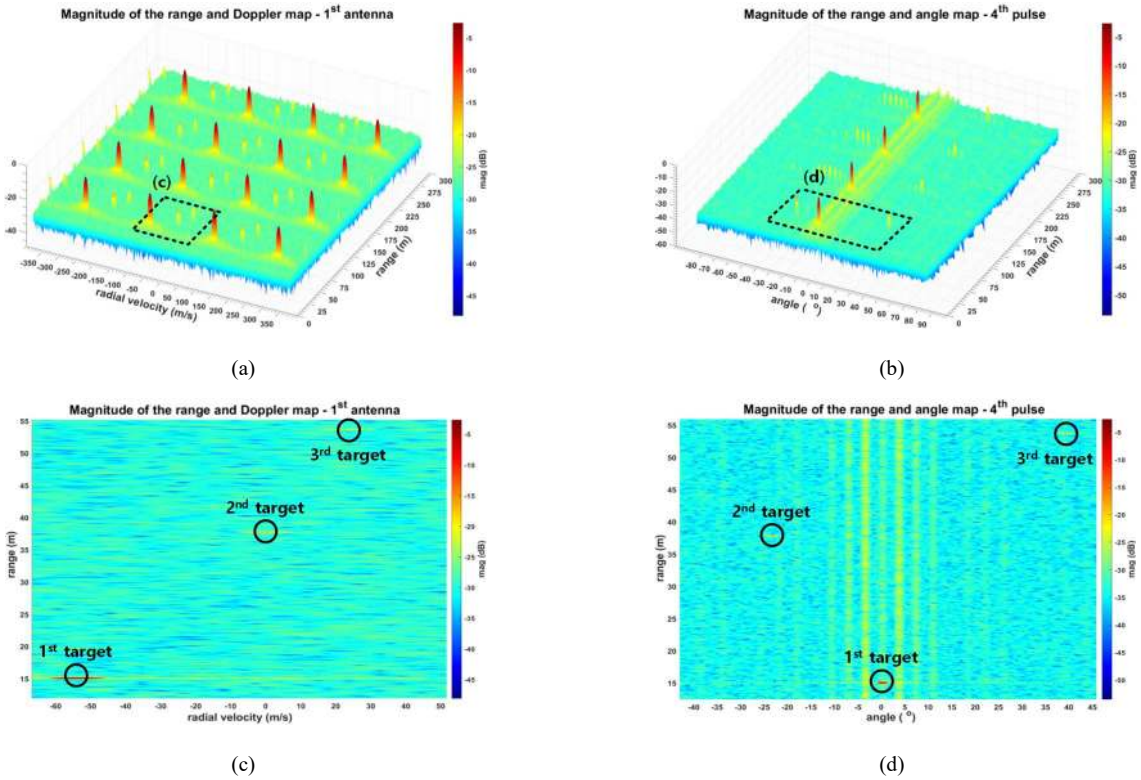

FIGURE 11. Simulation results of the 16 TXs & 8 RXs MIMO OFDM radar with 4 x 4 DFT-coded frequency-domain MIMO and 4 x 4 DFT-coded time-domain MIMO: (a) range-Doppler map of a 3D view, (b) range-angle map of a 3D view, (c) range-Doppler map of a 2D view in detail (the dotted rectangle in (a)), and (d) range-angle map of a 2D view in detail (the dotted rectangle in (b)).

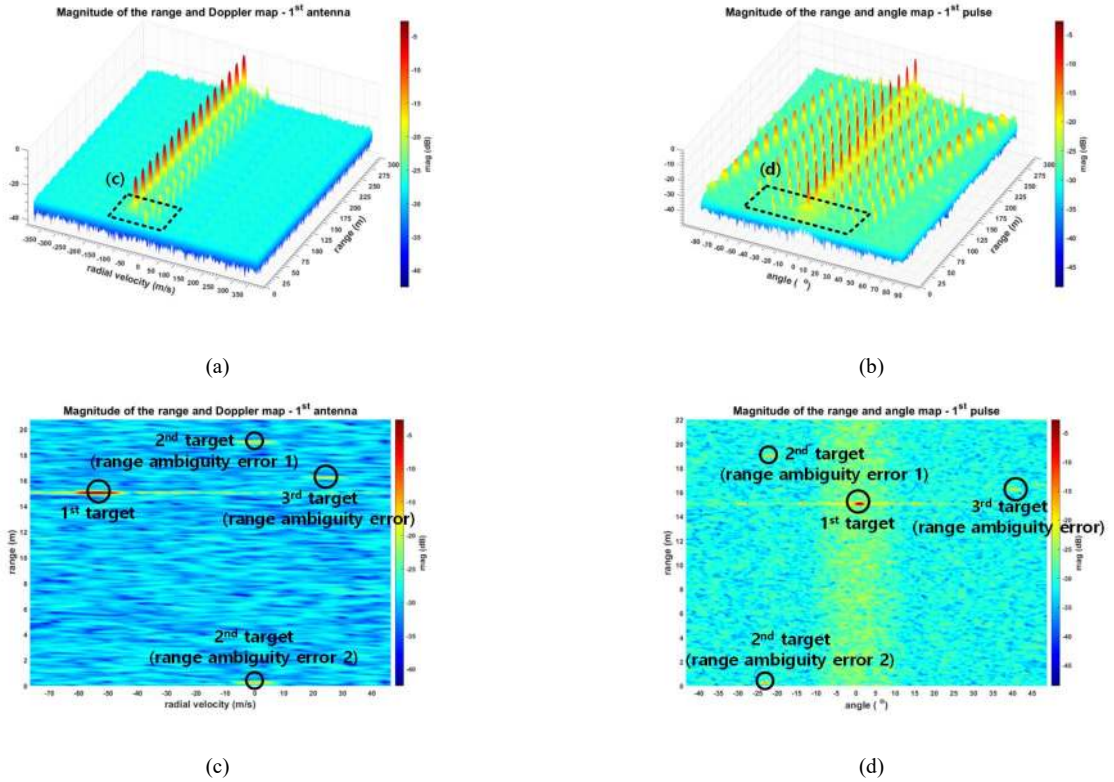

FIGURE 12. Simulation results of the 16 TXs & 8 RXs MIMO OFDM radar with the spectrally interleaved MIMO: (a) range-Doppler map of a 3D view, (b) range-angle map of a 3D view, (c) range-Doppler map of a 2D view in detail (the dotted rectangle in (a)), and (d) range-angle map of a 2D view in detail (the dotted rectangle in (b)).

TABLE 4. RMSE of the range, velocity, and angle information for each target with the simulation of two multiplexing methods

Multiplexing methods			RMSE of target range (m)			RMSE of target velocity (m/s)			RMSE of target angle (°)		
			1st target	2nd target	3rd target	1st target	2nd target	3rd target	1st target	2nd target	3rd target
Spectrally interleaved MIMO			0.019	*1 37.499	*2 37.502	0.025	0.015	0.019	1.315	0.112	1.857
DFT-coded Time-and-frequency hybrid MIMO	Hybrid ratio	2:8	0.019	0.010	0.012	*** 94.939	0.015	0.019	0.014	0.031	0.053
		8:2	0.017	**1 37.500	**2 37.501	0.023	0.016	0.018	0.013	0.030	0.051
		4:4	0.018	0.010	0.012	0.024	0.016	0.019	0.014	0.030	0.052

*1 with the presence of range ambiguity (0.25 m = 37.75 m – 2·18.75 m).
*2 with the presence of range ambiguity (16.2 m = 53.7 m – 2·18.75 m).
**1 with the presence of range ambiguity (0.25 m = 37.75 m – 37.5 m).
**2 with the presence of range ambiguity (16.2 m = 53.7 m – 37.5 m).
*** with the presence of velocity ambiguity (40.94 m/s = -54 m/s + 2·47.47 m/s).

Conversely, in Fig. 10, the first is at the maximum unambiguous velocity but the second and third targets are not in the maximum unambiguous range. Finally, in Fig. 11, all targets are in the maximum unambiguous range under the maximum unambiguous velocity. On the other hand, as shown in Fig. 12, the severe range ambiguity problem arises when the only spectrally interleaved MIMO is used for the same simulation.

As can be seen from the range-angle maps in Figs. 9 to 11, the angle information of each target is also accurate regardless of the corresponding range information so that the results are consistent with the proposed DFT-coded frequency-domain MIMO scheme. Whereas, the range-dependent angle errors are shown in the range-angle map from Fig. 12 for the case of the spectrally interleaved MIMO. The angle error of each target shows the dependency of the range ambiguity as described in (27).

C. PERFORMANCE ANALYSIS AND DISCUSSION

To compare the proposed multiplexing method with the conventional spectrally interleaved MIMO method, the target positions are estimated. For different cases of the uniformly distributed random payload data of 16-QAM, Monte Carlo simulations with the parameters shown in Table 2 are performed and the root mean square errors (RMSE) of range, velocity, and angle information for each target from Table 3 are obtained. $RMSE_{\mathrm{R},k}$, the RMSE for range information of the k^{th} target is defined as,

$$RMSE_{\mathrm{R},k} = \sqrt{\frac{\sum_{g=1}^{G}\left(\hat{R}_{g,k}-R_k\right)^2}{G}}\ , \tag{29}$$

where $\hat{R}_{l,k}$ is an estimate of the range, R_k is the real value, and $G = 100$ is the number of Monte Carlo simulations. To obtain $\hat{R}_{g,k}$ accurately, center-of-gravity (COG) based two-dimensional peak detection algorithm [48] is applied along the range profile on range-Doppler maps and range-angle maps. $RMSE_{\mathrm{v},k}$ and $RMSE_{\mathrm{a},k}$, the RMSEs for velocity and angle information of the k^{th} target, respectively, are obtained in the same way as above. The results of RMSEs for each multiplexing method are summarized in Table 4.

$RMSE_{\mathrm{R},k}$ and $RMSE_{\mathrm{v},k}$ of the spectrally interleaved MIMO and the proposed hybrid MIMO are similar except for the presence of range and Doppler ambiguities. For the spectrally interleaved MIMO case, $RMSE_{\mathrm{R},1}$ and $RMSE_{\mathrm{R},2}$ converge to twice the unambiguous range. In both of the results, $p'_{\mathrm{r},1}$ and $p'_{\mathrm{r},2}$ which are described in (19) equal to two, respectively. In a similar way, $RMSE_{\mathrm{R},1}$ and $RMSE_{\mathrm{R},2}$ of the proposed hybrid MIMO with the hybrid multiplexing ratio of 8 : 2 converge to one time the unambiguous range. Thus, $p'_{\mathrm{r},1}$ and $p'_{\mathrm{r},2}$ equal to one in this simulation, respectively. In terms of $RMSE_{\mathrm{v},1}$ for the proposed hybrid MIMO with the hybrid ratio of 2 : 8, it converges to twice the unambiguous velocity. In this result, $p'_{\mathrm{v},1}$ which is described in (21) equals to one.

Meanwhile, $RMSE_{\mathrm{R},k}$ and $RMSE_{\mathrm{v},k}$ for a fast moving target such as the 1st target in the simulations are getting worse than those of the other targets in both of the multiplexing methods due to the range-Doppler coupling. This coupling effect is approximated in (8) during the radar signal processing.

In terms of $RMSE_{\mathrm{a},k}$, the result of the spectrally interleaved MIMO is much worse than that of the proposed DFT-coded time-and-frequency hybrid MIMO. This is due to the range-angle coupling in the spectrally interleaved MIMO method. In addition, the range-dependent angle error appears differently for each target depending on how close the target is located at the integral multiple distances of the unambiguous range. Thus, $RMSE_{\mathrm{a},2}$ is lower than $RMSE_{\mathrm{a},1}$ in this simulation. However, $RMSE_{\mathrm{a},k}$ of the DFT-coded hybrid MIMO case is not affected by range and Doppler ambiguities. Therefore, it is expected that the range and Doppler ambiguity problems in a MIMO OFDM radar are solved by adaptively controlling the hybrid ratio of the proposed hybrid multiplexing method.

In summary, the proposed hybrid multiplexing method has the following advantages with a large number of transmitters in a MIMO OFDM radar system. It can operate without loss of the OFDM signal bandwidth and without loss of processing gain obtained from its use of many TXs. Furthermore, the proposed time-and-frequency hybrid multiplexing method does not affect the range, Doppler, and angular resolutions of an OFDM radar in spite of the changes of hybrid multiplexing ratio from the simulation results. In terms of the range resolution which is related to BW_{OFDM} of a radar system, it can be maintained regardless of the size of $N_{\mathrm{TX,fs}}$. Another, in terms of the Doppler resolution which is related to the CPI $\left(= M \cdot T_{\mathrm{radar\ pulse}}\right)$ of a radar system, it can be also maintained regardless of the size of $N_{\mathrm{TX,ts}}$. The other, in terms of the angular resolution which is related to the aperture size of a VRA for a MIMO radar system, it can be maintained regardless of the hybrid multiplexing ratios ($N_{\mathrm{TX,fs}} : N_{\mathrm{TX,ts}}$).

Moreover, the optimal maximum unambiguous range and velocity become negotiable properties of the radar, which are determined by selecting the hybrid multiplexing ratio without a change of the hardware configuration. To detect rapidly moving short-distance targets, the required maximum unambiguous velocity can be maximized by increasing the frequency-domain multiplexing ratio. On the other hand, to detect slow-moving long-distance targets, the required maximum unambiguous range can be maximized by increasing the time-domain multiplexing ratio.

V. CONCLUSION

A DFT-coded time-and-frequency hybrid MIMO multiplexing technique has been proposed for a MIMO OFDM radar system with many TXs to ensure a large aperture size with a virtual receive array. Orthogonality of the TXs is secured by applying DFT matrices to the transmitting signal in both the frequency-space and time-space domains. Typically, two kinds of multiplexing methods provide their own advantages and limitations. It has been shown that the hybrid multiplexing method mitigates performance limits by using their advantages, which is otherwise inevitable with many TXs. Since the hybridizing ratio of the two multiplexing methods determines the maximum unambiguous range and velocity of the MIMO OFDM radar system, it can adaptively improve certain performances over time-varying demands of radar operation environments. Also, the range-dependent angle errors which are the drawback of the conventional multiplexing method in a MIMO OFDM radar are not appeared in the proposed multiplexing method. A simulation platform using a numerical computing tool for the MIMO OFDM radar has been implemented, and the proposed multiplexing concept has also been presented.

REFERENCES

[1] S. Kueppers, H. Cetinkaya, R. Herschel, and N. Pohl, "A Compact 24 × 24 Channel MIMO FMCW Radar System Using a Substrate Integrated Waveguide-Based Reference Distribution Backplane," *IEEE Trans. on Microw. Theory Techn.*, vol. 68, no. 6, pp. 2124-2133, June 2020.

[2] V. Giannini et al., "9.2 A 192-Virtual-Receiver 77/79GHz GMSK Code-Domain MIMO Radar System-on-Chip," in *Proc. IEEE Intern. Solid- State Circuits Conf. - (ISSCC)*, Feb 2019, pp. 164-166.

[3] A. Ganis et al., "A Portable 3-D Imaging FMCW MIMO Radar Demonstrator With a 24 x 24 Antenna Array for Medium-Range Applications," *IEEE Trans. on Geosc. Remote Sensing*, vol. 56, no. 1, pp. 298-312, Jan. 2018.

[4] F. Schwartau et al., "Modular Wideband High Angular Resolution 79 GHz Radar System," in *Proc. German Microw. Conf. (GeMiC)*, Mar. 2019, pp. 194-197.

[5] F. Roos et al., "Comparison of 2D and 3D Compressed Sensing for High-Resolution TDM-MIMO Radars," in *Proc. Europ. Radar Conf. (EuRAD)*, Oct. 2019, pp. 253-256.

[6] J. Konishi, S. Ohashi, H. Yamada, Y. Yamaguchi, and M. Hiramoto, "Resolution enhancement for MIMO radar by using Khatri-Rao product virtual array processing," in *Proc. Intern. Symp. Antenna Prop. (ISAP)*, Oct. 2017, pp. 1-2.

[7] J. Zhao, Y. Liu, K. Huo, X. Zhang, and B. Xiao, "A Novel High-Resolution Imaging Method Using Reduced-Dimension Beamspace Unitary MUSIC for OFDM-MIMO Radar," *IEEE Access*, vol. 8, pp. 43676-43689, Feb. 2020.

[8] B. P. Ginsburg et al., "A multimode 76-to-81GHz automotive radar transceiver with autonomous monitoring," in *Proc. IEEE Intern. Solid - State Circuits Conf. - (ISSCC)*, Feb 2018, pp. 158-160.

[9] M. Kucharski et al., "A scalable 79-GHz radar platform based on single-channel transceivers," *IEEE Trans. on Microw. Theory Techn.*, vol. 67, no. 9, pp. 3882-3896, Sep. 2019.

[10] H. J. Ng, R. Hasan, and D. Kissinger, "A scalable four-channel frequency-division multiplexing MIMO radar utilizing single-sideband delta–sigma modulation," *IEEE Trans. on Microw. Theory Techn.*, vol. 67, no. 11, pp. 4578-4590, Nov. 2019.

[11] A. Och, C. Pfeffer, J. Schrattenecker, S. Schuster, and R. Weigel, "A Scalable 77 GHz Massive MIMO FMCW Radar by Cascading Fully-Integrated Transceivers," in *Proc. Asia-Pacific Microw. Conf. (APMC)*, Nov 2018, pp. 1235-1237.

[12] J. Overdevest, F. Jansen, F. Uysal, and A. Yarovoy, "Doppler Influence on Waveform Orthogonality in 79 GHz MIMO Phase-Coded Automotive Radar," *IEEE Trans. on Vehic. Techn.*, vol. 69, no. 1, pp. 16-25, Jan. 2020.

[13] C. Dahl, I. Rolfes, and M. Vogt, "Comparison of virtual arrays for MIMO radar applications based on hexagonal configurations," in *Proc. Europ. Radar Conf. (EuRAD)*, Sep. 2015, pp. 417-420.

[14] Y. Lin, Y. Fu, and S. Yang, "A Crossed Switching Scheme Applied to a TDM FMCW MIMO Radar," in *Proc. IEEE MTT-S Intern. Wireless Symp. (IWS)*, May 2019, pp. 1-3.

[15] J. Bechter, F. Roos, and C. Waldschmidt, "Compensation of Motion-Induced Phase Errors in TDM MIMO Radars," *IEEE Microw. Wireless Comp. Letters*, vol. 27, no. 12, pp. 1164-1166, Dec. 2017.

[16] X. Hu, Y. Li, M. Lu, Y. Wang, and X. Yang, "A Multi-Carrier-Frequency Random-Transmission Chirp Sequence for TDM MIMO Automotive Radar," in *IEEE Trans. on Vehic. Techn.*, vol. 68, no. 4, pp. 3672-3685, April 2019.

[17] R. Feger, C. Pfeffer, and A. Stelzer, "A frequency-division MIMO FMCW radar system using delta-sigma-based transmitters," in *Proc. IEEE MTT-S Intern. Microw. Symp. (IMS)*, June 2014, pp. 1-4.

[18] W. Wang, H. C. So, and H. Shao, "Nonuniform Frequency Diverse Array for Range-Angle Imaging of Targets," *IEEE Sensors Journal*, vol. 14, no. 8, pp. 2469-2476, Aug. 2014.

[19] S. Li, L. Zhang, N. Liu, J. Zhang, and S. Zhao, "Range-angle dependent detection for FDA-MIMO radar," in *Proc. CIE Intern. Conf. Radar*, Oct. 2016, pp. 1-4.

[20] H. A. Gonzalez, C. Liu, B. Vogginger, and C. G. Mayr, "Doppler Ambiguity Resolution for Binary-Phase-Modulated MIMO FMCW Radars," in *Proc. Intern. Radar Conf.*, Sep. 2019, pp. 1-6.

[21] A. Santra, A. R. Ganis, J. Mietzner, and V. Ziegler, "Ambiguity function and imaging performance of coded FMCW waveforms with fast 4D receiver processing in MIMO radar," *Digital Signal Processing*, vol. 97, p. 102618, Nov. 2019.

[22] F. Uysal, "Phase-Coded FMCW Automotive Radar: System Design and Interference Mitigation," *IEEE Trans. on Vehic. Techn.*, vol. 69, no. 1, pp. 270-281, Jan. 2020.

[23] Z. Wang, F. Tigrek, O. Krasnov, F. Van Der Zwan, P. Van Genderen, and A. Yarovoy, "Interleaved OFDM Radar Signals for Simultaneous Polarimetric Measurements," *IEEE Trans. Aerosp. Electr. Syst.*, vol. 48, no. 3, pp. 2085-2099, July 2012.

[24] C. Sturm, Y. L. Sit, M. Braun, and T. Zwick, "Spectrally interleaved multi-carrier signals for radar network applications and multi-input multi-output radar," *IET Radar, Sonar & Navig.*, vol. 7, no. 3, pp. 261-269, March 2013.

[25] Y. L. Sit and T. Zwick, "Automotive MIMO OFDM radar: Subcarrier allocation techniques for multiple-user access and DOA estimation," in *Proc. Europ. Radar Conf.*, Oct. 2014, pp. 153-156.

[26] D. Kuswidiastuti, M. Rizky, P. H. Mukti, and G. Hendrantoro, "MIMO radar waveform design using interleaved-OFDM technique," in *Proc. IEEE Intern. Conf. Comm., Netw. Satell. (COMNETSAT)*, Dec. 2016, pp. 53-59.

[27] Y. Lin, T. Lee, Y. Pan, and K. Lin, "Low-Complexity High-Resolution Parameter Estimation for Automotive MIMO Radars," *IEEE Access*, vol. 8, pp. 16127-16138, July 2019.

[28] T. Multerer, U. Prechtel, M. Vossiek, and V. Ziegler, "Systematic Phase Correction for Direction-of-Arrival Estimation in Spectrally Interleaved OFDM MIMO Radar," *IEEE Trans. on Microw. Theory Techn.*, vol. 67, no. 11, pp. 4570-4577, Nov. 2019.

[29] B. Nuss, L. Sit, M. Fennel, J. Mayer, T. Mahler, and T. Zwick, "MIMO OFDM radar system for drone detection," *in Proc. Intern. Radar Symp. (IRS)*, June 2017, pp. 1-9.
[30] C. Sturm, E. Pancera, T. Zwick, and W. Wiesbeck, "A novel approach to OFDM radar processing," in *Proc. IEEE Nation. Radar Conf.*, no. 3, Jun. 2009, pp. 9-12.
[31] T. Tian, T. Zhang, G. Li and, T. Zhou, "Mutual Information-Based Power Allocation and Co-Design for Multicarrier Radar and Communication Systems in Coexistence," *IEEE Access*, vol. 7, pp. 159300-159312, Nov. 2019.
[32] C. Shi, F. Wang, S. Salous, and J. Zhou, "Joint Subcarrier Assignment and Power Allocation Strategy for Integrated Radar and Communications System Based on Power Minimization," *IEEE Sensors Journal*, vol. 19, no. 23, pp. 11167-11179, Dec. 2019.
[33] I. Podkurkov, J. Zhang, A. F. Nadeev and, M. Haardt, "Efficient Multidimensional Wideband Parameter Estimation for OFDM Based Joint Radar and Communication Systems," *IEEE Access*, vol. 7, pp. 112792-112808, July 2019.
[34] C. Shi, F. Wang, S. Salous, and J. Zhou, "Low Probability of Intercept-Based Optimal OFDM Waveform Design Strategy for an Integrated Radar and Communications System," *IEEE Access*, vol. 6, pp. 57689-57699, Oct. 2018.
[35] A. Basireddy and H. Moradi, "OFDM Waveform Design for Interference Resistant Automotive Radars," *IEEE Sensors Journal*, vol. 21, no. 14, pp. 15670-15678, July 2021.
[36] L. G. d. Oliveira, M. B. Alabd, B. Nuss, and T. Zwick, "Range Association and Fusion in a Network of Single-Channel Monostatic OFDM Radars," in *Proc. IEEE MTT-S Intern. Conf. Microw. for Intell. Mobil. (ICMIM)*, Nov. 2020, pp. 1-4.
[37] D. Werbunat, B. Meinecke, B. Schweizer, J. Hasch, and C. Waldschmidt, "OFDM-Based Radar Network Providing Phase Coherent DOA Estimation," *IEEE Trans. on Microw. Theory Techn.*, vol. 69, no. 1, pp. 325-336, Jan. 2021.
[38] Z. Zhao, X. Zhou, S. Zhu, and S. Hong, "Reduced Complexity Multipath Clutter Rejection Approach for DRM-Based HF Passive Bistatic Radar," *IEEE Access*, vol. 5, pp. 20228-20234, Sep. 2017.
[39] X. Zhang, J. Yi, X. Wan, and Y. Liu, "Reference Signal Reconstruction Under Oversampling for DTMB-Based Passive Radar," *IEEE Access*, vol. 8, pp. 74024-74038, April 2020.
[40] L. Storrer et al., "Indoor tracking of multiple individuals with an 802.11ax Wi-Fi-based multi-antenna passive radar," *IEEE Sensors Journal*, Early Acess, July 2021.
[41] S. Zhu, R. Yang, X. Li, J. Zuo, D. Li, and Y. Ding, "An Optimizing Method of OFDM Radar Communication and Jamming Shared Waveform Based on Improved Greedy Algorithm," *IEEE Access*, vol. 8, pp. 186462-186473, Oct. 2020.
[42] M. Temiz, E. Alsusa, and M. W. Baidas, "A Dual-Functional Massive MIMO OFDM Communication and Radar Transmitter Architecture," *IEEE Trans. on Vehic. Techn.*, vol. 69, no. 12, pp. 14974-14988, Dec. 2020.
[43] Y. Liu, G. Liao, Y. Chen, J. Xu, and Y. Yin, "Super-Resolution Range and Velocity Estimations With OFDM Integrated Radar and Communications Waveform," *IEEE Trans. on Vehic. Techn.*, vol. 69, no. 10, pp. 11659-11672, Oct. 2020.
[44] J. B. Sanson, P. M. Tomé, D. Castanheira, A. Gameiro, and P. P. Monteiro, "High-Resolution Delay-Doppler Estimation Using Received Communication Signals for OFDM Radar-Communication System," *IEEE Trans. on Vehic. Techn.*, vol. 69, no. 11, pp. 13112-13123, Nov. 2020.
[45] S. Jeon et al., "W-Band FMCW MIMO Radar System for High-Resolution Multimode Imaging with Time- and Frequency-Division Multiplexing," *IEEE Trans. Geosc. Remote Sensing*, vol. 58, no. 7, pp. 5042-5057, July 2020.
[46] F. Yang, F. Xu, X. Yang, and Q. Liu, "DDMA MIMO radar system for low, slow, and small target detection," *The Journal of Engin.*, vol. 2019, no. 19, pp. 5932-5935, Oct. 2019.
[47] D. J. Rabideau, "Doppler-offset waveforms for MIMO radar," in *Proc. IEEE Radar Conf.*, May 2011, pp. 965-970.
[48] Lübbert, Urs, *Target Position Estimation with a Continuous Wave Radar Network*. Hamburg-Harburg, Germany: Göttingen, Cuvillier, 2005, pp. 46–48.

JUNSEUK SUH (S'17) was born in Seoul, South Korea, in 1989. He received his B.S. degree in electronic and electrical engineering from Sungkyunkwan University, Suwon, South Korea, in 2014, and his M.S. degree in electrical engineering from the Korea Advanced Institute of Science and Technology, Daejeon, South Korea, in 2016, where he is currently pursuing a PhD. His current research interests include designing radar systems, radar applications, and the RF integrated circuits for radar applications.

JUNGAH LEE (M'97) received her B.S. and M.S. degrees in electronics engineering from Seoul National University, Seoul, South Korea, in 1987 and 1989, respectively, and her PhD in electrical engineering from the University of Illinois at Urbana-Champaign, USA, in 1997. Her research interests are signal processing, wireless communication systems, and synthetic aperture radar imaging. Between 2012 and 2015, she was with Samsung Electronics, Suwon, Korea, as the Senior Vice President of Advanced Technology Group. She led technology, strategy and engagement with leading customers and partners. She led development of Samsung's advanced 4G radio system, edge computing and network analytics solution CognitiV. Prior to joining Samsung Electronics, she was with Lu-cent Technologies – Bell Labs (currently Nokia) as a Distinguished Member of Technical Staff. She made significant contributions in core technology, design and standardization of 3G and 4G systems. She is a recipient of Bell-Labs President's Gold Award and holds more than 40 international patents. She is a founder and CEO of Aura Intelligent Systems, Inc., a Boston based company building imaging radar system. She was the Head of Advanced Technology at Altiostar Networks, USA, a disruptive mobile system provider, where she took Altiostar's vRAN to global 5G standards.

GYE-TAE GIL (M'04) received his B.S. degree in electronic communication engineering from Hanyang University, Seoul, South Korea, in 1989, and his M.S. degree and PhD in electrical engineering from the Korea Advanced Institute of Science and Technology (KAIST), South Korea, in 1992 and 2004, respectively. Since 1991, he has been with the Research Center of Korea Telecom, and joined the KAIST Institute in 2013, where he is currently a Research Professor. His research interests are in the area of communication signal processing, which includes synchronization, interference cancellation, and adaptive filter design. He is also interested in orbital angular momentum transmission, MIMO OFDM radar, and massive antenna technologies for cellular mobile communication systems.

SONGCHEOL HONG (S'87–M'88) received his B.S. and M.S. degrees in electronics engineering from Seoul National University, Seoul, South Korea, in 1982 and 1984, respectively, and his PhD in electrical engineering and computer science from the University of Michigan, Ann Arbor, MI, USA, in 1989. In 1997, he joined the EECS Department of Stanford University in Stanford, CA, USA, as a Visiting Professor. He worked with Samsung Microwave Semiconductor, Milpitas, CA, USA. He served as the Dean of Research Affairs and the Director of KI-IT Convergence with the Korea Advanced Institute of Science and Technology (KAIST), Daejeon, South Korea. He is currently a Professor with the School of Electrical Engineering of KAIST, where he is also a KT-Chaired Professor. He has authored or coauthored more than 300 technical papers and holds 150 patents. His current research interests include RFICs and RF CMOS PAs, especially in millimeter-wave ICs for 5G communications and radar systems.
Dr. Hong is currently a member of NAEK, KIEES, and KITE. He served as a Board member of Techno-park of Daejeon Metropolitan city. He served as the General Chair for RFIT 2017 supported by IEEE and the TPC Chair for APMC 2013 and GSMM 2014.